AFOSR TR. 81-0650

LEVEL II

USCIPI REPORT 1020

AD A105186

ENGINEERING

UNIVERSITY OF SOUTHERN CALIFORNIA

FINAL TECHNICAL REPORT

April 15, 1977 - April 14, 1981

NONLINEAR REAL-TIME OPTICAL SIGNAL PROCESSING

A.A. Sawchuk, Principal Investigator
T.C. Strand, and A.R. Tanguay, Jr.

June 30, 1981

Department of Electrical Engineering
Image Processing Institute
University of Southern California
Los Angeles, California 90007

DTIC
SELECTED
OCT 7 1981
D

IPI

81 10 5 025

REPORT DOCUMENTATION PAGE	READ INSTRUCTIONS BEFORE COMPLETING FORM

1. REPORT NUMBER	2. GOVT ACCESSION NO.	3. RECIPIENT'S CATALOG NUMBER
AFOSR-TR-81-0650	AD-A105186	

4. TITLE (and Subtitle)	5. TYPE OF REPORT & PERIOD COVERED
NONLINEAR REAL-TIME OPTICAL SIGNAL PROCESSING	Final Report 4/15/77 - 4/14/81
	6. PERFORMING ORG. REPORT NUMBER USCIPI Report 1020

7. AUTHOR(s)	8. CONTRACT OR GRANT NUMBER(s)
A.A. Sawchuk, T.C. Strand and A.R. Tanguay, Jr	AFOSR-77-3285

9. PERFORMING ORGANIZATION NAME AND ADDRESS	10. PROGRAM ELEMENT, PROJECT, TASK AREA & WORK UNIT NUMBERS
Department of Electrical Engineering Image Processing Institute University of Southern California Los Angeles, CA 90007	61102F 2305/B1

11. CONTROLLING OFFICE NAME AND ADDRESS	12. REPORT DATE
Air Force Office of Scientific Research Bldg. 410, Bolling AFB Washington, D.C. 20332	June 30, 1981
	13. NUMBER OF PAGES 82 pages

14. MONITORING AGENCY NAME & ADDRESS(if different from Controlling Office)	15. SECURITY CLASS. (of this report)
as above	UNCLASSIFIED
	15a. DECLASSIFICATION DOWNGRADING SCHEDULE

16. DISTRIBUTION STATEMENT (of this Report)

Approved for public release;
distribution unlimited.

17. DISTRIBUTION STATEMENT (of the abstract entered in Block 20, if different from Report)

18. SUPPLEMENTARY NOTES

19. KEY WORDS (Continue on reverse side if necessary and identify by block number)

Optical information processing
Nonlinear optical processing
Real-time optical processing
Optical computing

20. ABSTRACT (Continue on reverse side if necessary and identify by block number)

The results of a four year research program in nonlinear real-time optical signal processing are described. The goal of the program was to extend fast parallel nonlinear operations to optical processing systems with large time-bandwidth and space-bandwidth products. Real-time homomorphic and logarithmic filtering by halftone nonlinear processing has been achieved. A detailed analysis of degradation due to the finite gamma and other non-ideal effects of the recording medium has been completed along with an extensive study of techniques for precompensating these effects. Further improvements

DD FORM 1473 EDITION OF 1 NOV 65 IS OBSOLETE
1 JAN 73

in experimental work await a liquid crystal light valve (LCLV) or other
real-time spatial light modulator with a sharper threshold and better uni-
formity and repeatability. A direct nonlinear technique of real-time
parallel A/D conversion of an incoherent optical image has been developed.
A detailed theoretical analysis and modeling of liquid crystal devices
and associated photoconductors was completed, providing an excellent fit
to experimental data obtained on several devices provided by Hughes
Research Laboratories. These results have been used to make a flexible
multiple light valve system (MLVS) in which the form of the nonlinearity
can be varied. Variable-grating mode (VGM) liquid crystal devices that
perform local spatial frequency modulation as a function of the incident
intensity have been developed. These devices can be used for nonlinear
processing by selection and recombination of these spatial frequency
components. These devices have many interesting physical effects with
useful applications in both analog and numerical optical signal processing.
Preliminary theoretical modeling work to explain these effects is given,
and experimental implementation of binary combinatorial logic functions
with VGM devices has been demonstrated. The project was a joint effort
between the University of Southern California Image Processing Institute
(USCIPI) and the Hughes Research Laboratories (HRL), Malibu, California.

Accession For	
NTIS GRA&I	☒
DTIC TAB	☐
Unannounced	☐
Justification	

By	
Distribution/	
Availability Codes	
Dist	Avail and/or Special
A	

USCIPI Report 1020

FINAL TECHNICAL REPORT

April 15, 1977 - April 14, 1981

NONLINEAR REAL-TIME OPTICAL SIGNAL PROCESSING

A.A. Sawchuk, Principal Investigator
T.C. Strand, and A.R. Tanguay, Jr.

June 30, 1981

Department of Electrical Engineering
Image Processing Institute
University of Southern California
Los Angeles, California 90007

DTIC
ELECTE
OCT 7 1981
D

D

TABLE OF CONTENTS

ABSTRACT

The results of a four year research program in nonlinear real-time optical signal processing are described. The goal of the program was to extend fast parallel nonlinear operations to optical processing systems with large time-bandwidth and space-bandwidth products. Real-time homomorphic and logarithmic filtering by halftone nonlinear processing has been achieved. A detailed analysis of degradation due to the finite gamma and other non-ideal effects of the recording medium has been completed along with an extensive study of techniques for precompensating these effects. Further improvements in experimental work await a liquid crystal light valve (LCLV) or other real-time spatial light modulator with a sharper threshold and better uniformity and repeatability. A direct nonlinear technique of real-time parallel A/D conversion of an incoherent optical image has been developed. A detailed theoretical analysis and modeling of liquid crystal devices and associated photoconductors was completed, providing an excellent fit to experimental data obtained on several devices provided by Hughes Research Laboratories. These results have been used to make a flexible multiple light valve system (MLVS) in which the form of the nonlinearity can be varied. Variable-grating mode (VGM) liquid crystal devices that perform local spatial frequency modulation as a function of the incident intensity have been developed. These devices can be used for nonlinear processing by

selection and recombination of these spatial frequency components. These devices have many interesting physical effects with useful applications in both analog and numerical optical signal processing. Preliminary theoretical modeling work to explain these effects is given, and experimental implementation of binary combinatorial logic functions with VGM devices has been demonstrated. The project was a joint effort between the University of Southern California Image Processing Institute (USCIPI) and the Hughes Research Laboratories (HRL), Malibu, California.

1.   RESEARCH OBJECTIVES AND PROGRESS

1.1 Introduction and Project Overview

This report summarizes the results of a four year research effort in performing nonlinear operations in optical signal processing and achieving operation in real time using various input transducers. This section contains an introduction, motivation for the work and an overview of the research program. A large number of publications, reports and presentations have resulted from this work. Some of these publications are reprinted here to provide a detailed discussion of various research areas. More recent research results are also summarized. The relationships between these research areas are described at the beginning of each section.

There is a great general need for systems which can perform fast, parallel multi-dimensional operations on signals with large time-bandwidth and space-bandwidth products. These needs arise in terminal guidance, nonlinear tracking and signal filtering, imaging radar systems, image processing, image target and pattern recognition and automated assembly [1]-[3]. In many of these applications, electronic analog and digital hardware is inadequate.

The parallel nature of optical systems and their inherently large space-bandwidth product has led to the development of many systems and techniques for optical information processing. A

fundamental difficulty with optical processing has been the limited range of operational "software" available [4]-[6]. Thus, general nonlinear operations such as logarithms, power laws, and limiters have been very hard to implement, while linear operations such as correlation, convolution, and filtering have been relatively easy. Many new techniques of signal processing and pattern recognition require nonlinear functions as part of their operation, and these functions have been achieved digitally, although in serial form [3]. Under this AFOSR program, the range of operations in optical processing has been greatly extended to include these nonlinear functions and many others such as A/D conversion and level slicing [7].

A second major difficulty of optical information processing is the problem of input and output [8]-[12]. Recent developments have simplified the output problem: television and solid-state devices are available to efficiently make use of the two-dimensional processed output. In many situations, the human eye or observer is the end user of the information, so that optical systems with their inherent two-dimensional nature are ideally suited to process pictorial information intended eventually for the human observer. The major difficulty lies with real-time input to optical processors. Flexible real-time optical input modulators which can convert electronic or image information into a form for input to a processing system are badly needed, and significant research over the last several years has made progress on certain aspects of this problem.

A final problem with traditional optical processors is that the computations are performed almost exclusively in an analog fashion. Another goal of this program has been to explore numerical optical computing using binary [13]-[24] or residue [25]-[31] arithmetic. In these systems, signals exist as discrete levels rather than as analog signals. This new approach holds much promise for the future if real-time processing speed, accuracy, and flexibility can be maintained.

Two papers [49,50] written by research personnel supported under this grant have been recently completed summarizing the state-of-the-art of all techniques of nonlinear optical processing. These papers contain extensive references. With nonlinear point functions, the three major techniques of nonlinear processing are: halftoning; intensity-to-spatial frequency conversion; and direct nonlinear processing using the inherent characteristics of image detectors and transducers. Application examples and real-time implementation of these techniques are described in the review papers. A brief summary of these methods is given in the next few paragraphs.

The halftone method of nonlinear processing is a two step procedure. The first step converts the continuous level two-dimensional input signal into a pulse-width modulated (ideally) binary input. This operation is exactly the halftone procedure used in the graphic arts to represent an image containing gray tones as a binary picture. The halftoning step

uses a mask transparency called a halftone screen along with a high contrast (ideally, a sharp threshold) photographic material or real-time coherent optical input transducer.

With both photographic or real-time halftoning, the second step of the process is Fourier filtering and recombination of diffraction components in a coherent optical system. The many variations of halftone screens and filtering procedures permit great flexibility in the nonlinear functions that can be achieved.

In the first part of this program, nonlinear coherent optical processing with halftone screens and real-time devices was emphasized [32]-[34], [42]. Certain fundamental limitations of this technique due to problems of hysteresis, nonuniformity, and lack of a threshold with the real-time devices have been identified. Although these effects can be precompensated by methods developed under this program [42], several new alternative techniques for nonlinear processing have been developed.

Another convenient method of obtaining point nonlinearities is through intensity-to-spatial frequency conversion. The idea is to encode each resolution element of an image with a grating structure where the period and/or the orientation of the grating is a function of the image intensity at the point in question. Assuming certain sampling requirements are met, each intensity level of interest is uniquely assigned to a different point in

Fourier space and all points with a given intensity in the image are assigned to the same point in Fourier space (assuming space-invariant operation is desired). Then a pure amplitude spatial filter can alter the relative intensity levels in an arbitrary way, and combination of the filtered components produces various nonlinear functions. Both continuous-level (analog) nonlinear functions and various numerical logic functions (binary or residue) are possible. This method relies on the behavior of variable-grating mode (VGM) liquid crystal real-time devices which have been developed under this AFOSR program.

Direct nonlinear optical functions can be achieved using the inherent transfer characteristics of an optical recording medium or real-time image transducer. With this type of nonlinear processing, there is no pulse-width modulation, intensity-to-spatial frequency conversion or other type of intermediate mechanism. Thus, these techniques offer the potential of simple systems that avoid the noise problems associated with many optical filtering techniques and have much less stringent space-bandwidth product requirements than systems which must modulate the input data. One drawback is that the flexibility of this technique is considerably more limited than the two previous methods.

The overall program has been a joint cooperative effort between the University of Southern California (USC) group and the

Hughes Research Laboratories (HRL) in Malibu, California. Each group has participated in the project together since its beginning in April 1977 and a separate progress report is being submitted by HRL as a companion to this report. Both groups have worked closely together in their particular areas of expertise toward the project goals.

HRL has made many modifications and developments in liquid crystal light valve (LCLV) technology as part of this project. The HRL group is one of the leaders in this technology and have developed an advanced, commercially available transducer for linear processing. Some of the techniques which have been studied include: a) modifying existing LCLVs to provide a sharp threshold (high gamma) and sharper toe and shoulder of the characteristic curve for use with halftone nonlinear processing; b) theoretically and experimentally studying liquid crystal devices with variable grating mode (VGM) characteristics; c) improving the uniformity and repeatability of existing devices to achieve certain halftone nonlinearities by precompensation; and, d) directly utilizing the nonlinear characteristics of modified LCLVs to achieve A/D conversion and other functions in incoherent systems.

1.2 Halftone Processing

In the first part of this program, nonlinear coherent optical processing with halftone screens and real-time devices was emphasized. The Ph.D. thesis of A. Armand [42] published as IPI Technical Report 880 contains the major results of this work. Several papers have been given [32]-[34] or are in preparation [43], [44] on this subject.

The most important point about halftone nonlinear processing is the pulse-width modulation process of copying the input through a halftone screen onto the real-time device. The device must ideally have a sharp threshold characteristic. A general analysis given in detail in Ref. [42] predicts the effects of the copying medium given a screen profile and diffraction order. Computer simulation is used to predict degradation of the input-output curves from the ideal. The results of this work are extensive [42],[47]-[48]; only a sample is given here.

For smooth monotonic nonlinear functions such as the logarithm, the main source of output degradation is the linear section of the t vs. D_{in} characteristic curve as shown in Fig. 1. The saturation regions where the slope of the curve is zero for low and high values of D_{in} have less effect on the performance. Figure 2 shows these effects. Figure 2(a) is the ideal two decade logarithmic response, where the horizontal axis is plotted on a normalized scale. Figure 2(b) shows the degraded response
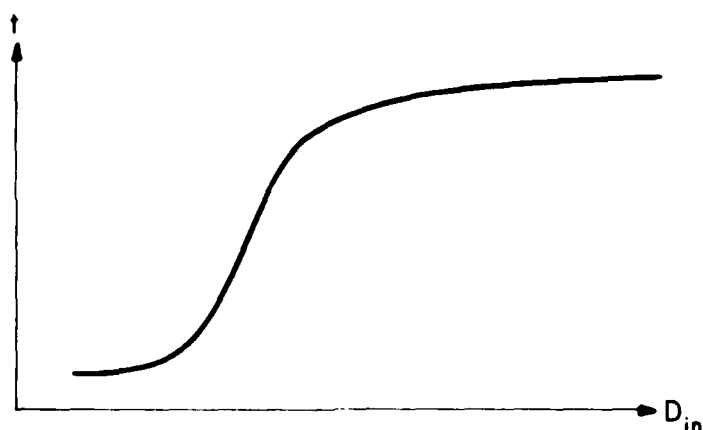
Figure 1.   Transmittance vs. input density for a general
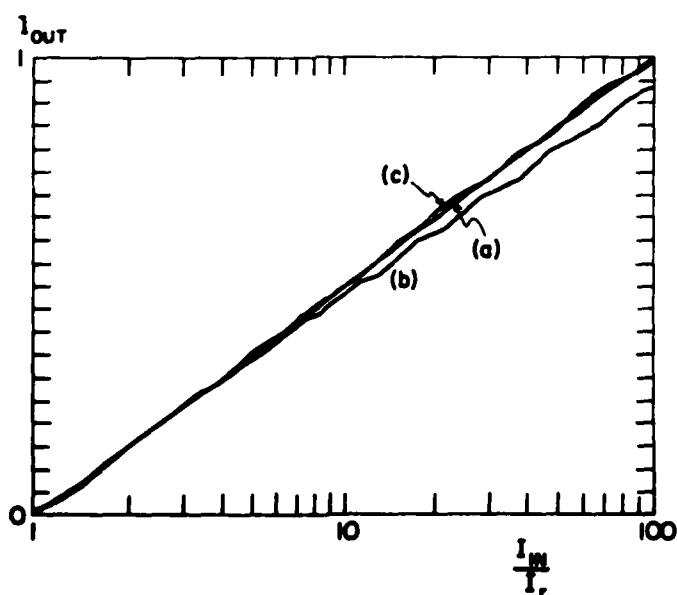   non-ideal recording system.

Figure 2.   Logarithmic function for a piecewise linear model
            of a recording medium with gamma = 3.0.   (a) Ideal.
            (b) Degraded.   (c) Optimized.

for a copying medium having a photographic gamma (slope of the linear part of the density vs. log exposure curve) of 3.0. The curve showing the degradation was computed using a piecewise linear model for the curve of the copy medium of Fig. 1, although any particular measured response curve can be used. In Fig. 2, the I_{out} response tends to fall below ideal for high values of normalized I_{in}.

For nonlinearities with sharp slope changes and sharp corners, such as the level slice function, the sharp rising and falling transitions have a reduced slope, and the sharp corners tend to become rounded. The reason for this is that sharp threshold functions completely rely on the thresholding characteristic of the copy medium to attain their sharp slope. This effect can be seen by comparing the ideal level slice shown in Fig. 3(a) with the degraded results shown in Fig. 3(b). Given a copy medium with a finite gamma greater than one, it is possible to increase the effective gamma by making a copy of the first halftoned image. The overall gamma of the process will increase and the threshold will be sharper. However, this procedure is clumsy and impractical for real-time implementation.

Given a non-ideal recording medium and a desired input-output curve, two methods are available to design an optimum halftone screen which produces the best fit to the desired nonlinear response. Both techniques begin with analytic expressions relating these functions [42]. The first method

analytically inverts the degrading equations. Although this
method is exact, it is currently restricted to certain monotonic
nonlinearities such as power law and exponential transformations,
and it is also restricted to a piecewise linear model for the
recording medium characteristic curve. Solution for more
complication models may be possible, but is analytically very
difficult.

In an alternative method, the halftone screen density
profile to be derived is assumed to be quantized. Optimum
quantized values are found by minimizing the difference between
desired and degraded outputs in the least-square sense. This
method can be used for any form of the recording medium
characteristic curve and any type of nonlinearity. In
application, the halftone screen is made on a plotting device
with discrete density levels, thus this procedure gives a good
practical solution.

The results of computer simulation of compensation for a
logarithmic function is shown in Fig. 2(c). In this simulation,
30 discrete points in the halftone screen density profile and
screen density values from 0 to 2 are assumed. The optimized
output curve is seen to approximate the ideal result in Fig. 2(a)
with much less error than before. Similar results for a level
slice function are shown in Fig. 3(c). Here the optimization
procedure is successful in improving the fit to the ideal, but
cannot increase the finite slope on the sharp transitions at the

boundaries of the degraded response. Details of these procedures and many additional simulation results are given in the references [42].

Some experimental results on real-time nonlinear halftone processing with LVLVs are given here. Both logarithmic and level-slice functions have been attempted with a standard Hughes liquid crystal light valve (LCLV) suitable for linear incoherent-to-coherent optical conversion.

The LCLV exists in both electronically and optically controlled versions. The optical LCLV serves as a real-time incoherent-to-coherent converter. Incoherent light impinges on a photoconductor, which in turn changes the local electric field across a liquid crystal layer. The change in electric field alters the local birefringence of the liquid crystal material. This birefringence pattern can be read out as a spatial amplitude modulation by placing an analyzer in the output beam oriented orthogonal to the initial polarization of the readout beam. The readout illumination can be spatially coherent or incoherent, but must be temporally narrowband. Additional variations in the device response are possible by introducing a twist in the alignment of the liquid crystal molecules during device assembly. The LCLV device operates at television frame rates (approximately 30 ms. cycle time) and generally is designed to have a linear response over two decades of dynamic range. Many references that discuss construction and operational details are available

[11],[12].

To obtain a real-time logarithmic nonlinearity [42], the characteristic curves of a Hughes 45° twisted nematic LCLV were measured. Figure 4(a) is the original characteristic curve of the LCLV, showing that the device has a smooth curve approximately that of photographic film with a gamma of 2 to 3. Using this data, an optimum compensated discrete halftone screen was made. This halftone screen had a fundamental spatial frequency of 3 cycles/mm, and was designed to work in the zero diffraction order.

The experimental setup used is shown in Fig. 5. The continuous level input is placed in contact with the halftone screen and imaged onto the control surface of the LCLV with incoherent illumination. The LCLV is read out with coherent light between crossed polarizers and a pinhole spatial filter is placed in the zero order in the Fourier plane of the system. Figure 4(b) shows the response curve of the system with the halftone screen in place. The result approximates a logarithmic transfer function with less than 5% error over one decade and less than 10% error over two decades.

To test the effectiveness of the logarithmic filtering system in another experiment, two crossed multiplicatively combined Ronchi rulings were used as an input picture for the experimental setup of Fig. 5. The period of these rulings was approximately 3 mm, much higher than the halftone screen period
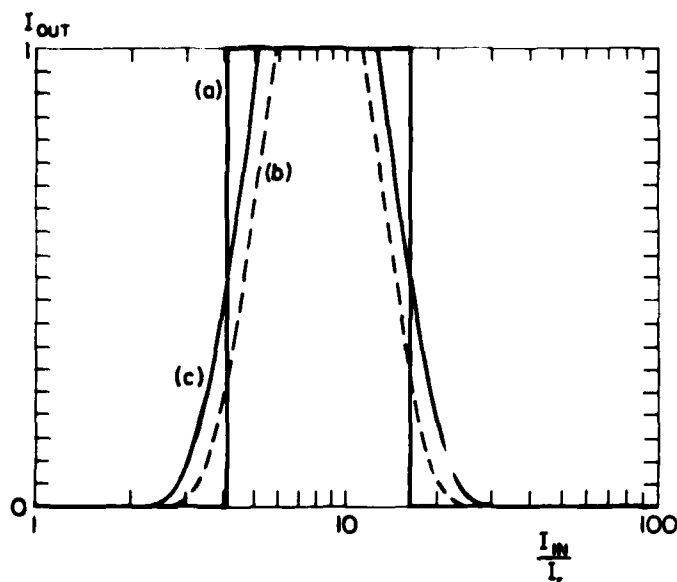
Figure 3. Level slice function for a piecewise linear model
of a recording medium with gamma = 3.0. (a) Ideal.
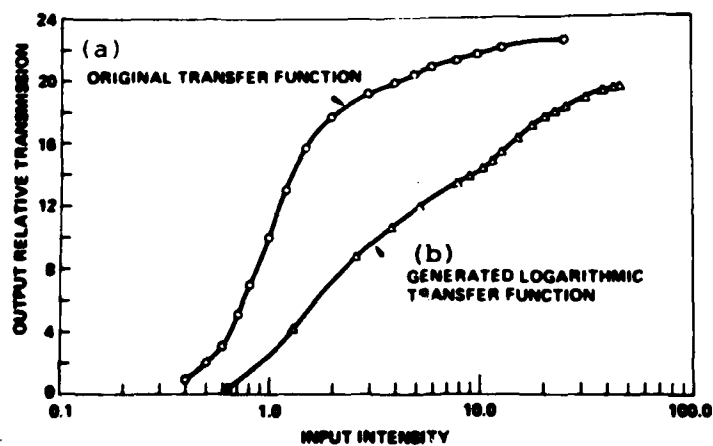(b) Degraded. (c) Optimized.

Figure 4. Liquid crystal characteristic curve. (a) Without
the halftone screen. (c) With halftone screen
designed to give a logarithmic response over two
decades.

of 0.33 mm. The spectrum in the filter plane is shown in Fig. 6(a). Next, the logarithm halftone screen was placed in contact with the rulings. The filter plane spectrum is shown in Fig. 6(b). The difference in Fourier spectra between multiplicatively combined gratings and additively combined grating obtained by real-time logarithmic filtering is as follows: the additive spectrum components lie only on the x and y axes (at 45° and 135°, respectively from the horizontal axis) around the zeroth diffraction order in the frequency domain while the multiplicative spectrum contains cross-term off-axis components. Figure 6 also shows the higher diffraction orders that arise due to the halftone screen. For simple logarithmic processing, these higher orders would be eliminated by spatial filtering.

The system has also been applied to an image filtering problem. For this experiment a picture with multiplicative noise was generated. The goal was to eliminate the multiplicative noise by homomorphic filtering; i.e., a sequence of a logarithmic transformation followed by filtering and then an exponential transformation [42]. The final exponential transformation is not essential in demonstrating noise reduction and was not included in the following experiments. The noise generated for this experiment models that of a push-broom scanner that scans six lines at a time with six independent detectors. Any variation in the sensitivity or gain along the row of detectors gives rise to a periodic six-bar noise structure across the image. This effect
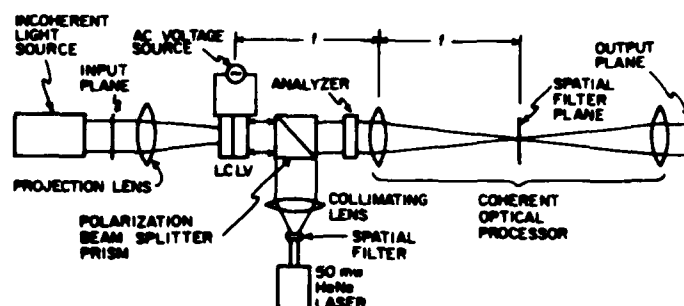
Figure 5.   Experimental setup for real-time halftone processing with a LCLV.

(a)

(b)

0th   1st   2nd
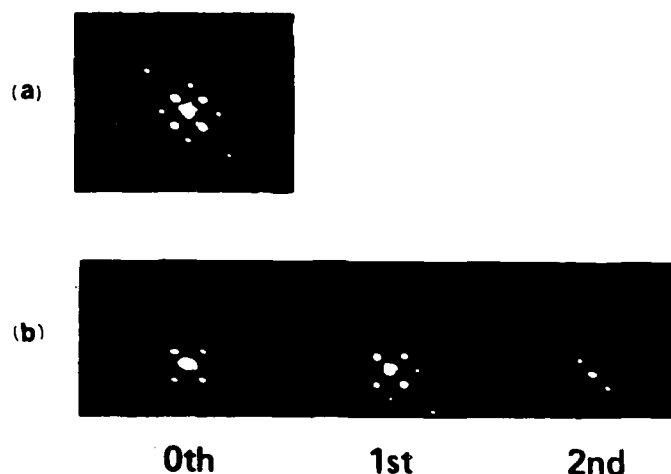
Figure 6.   Real-time logarithmic processing with a halftone screen and a LCLV. (a) Fourier transform of two crossed gratings imaged on the LCLV with no half-tone screen. The grating spectra are convolved with one another. (b) Fourier transform of crossed gratings with the halftone screen. In the zeroth order, the off-axis terms have been eliminated indicating the grating spectra are not convolved with one another. Note: the x-y axes are 45° and 135°, respectively from the horizontal axis.

is shown in Fig. 7(a). The density range of the image with the simulated scanner noise was 2.0D. This was chosen to match the 100:1 operating range of the halftone screen.

The noisy image was sandwiched with the halftone screen and imaged with incoherent illumination onto the LCLV. The resultant image was read out with a HeNe laser. A spatial filter was placed in the Fourier plane of the system to select a single (zeroth) diffraction order in the halftone spectrum. Since the screen effectively performs a logarithmic transformation, the pattern in the zeroth diffraction order of the Fourier plane consisted of the sum of the image diffraction pattern and the push-broom scanner diffraction pattern. The scanner diffraction pattern consisted of a series of isolated diffraction orders which could be filtered out without significantly degrading the image. Thus in the output plane the image is reconstructed without the multiplicative noise. This is shown in Fig. 7(b). Without the logarithmic transformation, the noise and image spectra would have been convolved with one another making them impossible to separate.

These experiments demonstrate the feasibility of performing real-time nonlinear filtering for smooth functions using an LCLV or other real-time device. A real-time level slice experiment has also been performed with a standard linear 45° twisted nematic LCLV [48] and the results are comparable to the degraded level slice work shown in the simulations of Fig. 3(b).

(a)

(b)

Figure 7. Real-time homomorphic filtering. (a) Input image
is a face with simulated push-broom scanner noise.
Overall density range is 2.0 D. (b) Homomorphic
filtered output.

The fundamental limitation of the halftone process is the optical threshold function which must be performed by the real-time device. Although the compensation procedures are effective for smooth nonlinearities such as logarithms and power laws, the thresholding is absolutely essential for functions with sharp jumps such as level slicing or A/D conversion. Until much sharper thresholds are available in real-time devices, halftone processing will not be effective for functions with step discontinuities. The threshold functions turns out to be much more significant for other nonlinear processing techniques besides halftoning. Direct nonlinear processing and binary numerical processing depend heavily on the existence of thresholds. Thus, the study of general parallel real-time thresholding techniques deserves additional future work. Additional problems of repeatability, temperature sensitivity and nonuniform response in existing LCLVs have also become evident in very recent experimentation. Methods of overcoming these problems continue to be studied in follow-on research.

1.3 <u>Direct</u> <u>Nonlinear</u> <u>Processing</u>

The direct nonlinear method of achieving real-time parallel A/D conversion described in a previous Annual Report [7] and in the Ph.D. thesis of A. Armand [42] has been published in <u>Optics</u> <u>Letters</u> [36]. This publication is reprinted here. The technique has been limited to three-bit resolution by the aperiodicity, nonuniformity and nonrepeatability of the pure birefringent LCLV used. No further work on A/D applications of direct processing is planned unless some of these difficulties can be overcome. However, recent work by Collins, et al. [45] has demonstrated the use of birefringent LCLVs for optical logic, in an application similar to the variable-grating-mode (VGM) logic described in subsequent sections.

Real-time parallel optical analog-to-digital conversion

A. Armand, A. A. Sawchuk, and T. C. Strand

Department of Electrical Engineering, Image Processing Institute University of Southern California, Los Angeles, California 90007

D. Boswell and B. H. Soffer

Hughes Research Laboratories, 3011 Malibu Canyon Road, Malibu, California 90265

A technique for optically performing parallel analog-to-digital conversion on incoherent two-dimensional inputs at real-time rates is described. The system uses a birefringent optical real-time input transducer combined with a detector array and optical thresholding. Quantization and bit plane outputs are produced in parallel without scanning. An experimental system with three-bit accuracy is described.

The process of analog-to-digital (A/D) conversion is the representation of continuous analog information in sampled and quantized form. For one-dimensional signals, any coding procedure that assigns to each signal value a group of digits (bits) performs such an operation. For digital processing of multidimensional signals and images, the sampling, quantization, and digitization must be performed on an array of data. We describe here a technique of real-time incoherent nonlinear optical processing that performs two-dimensional A/D conversion of images or other page-organized data in parallel without the need for scanning. The method relies on the nonlinear characteristics of real-time optical input devices, such as the Hughes liquid-crystal light valve (LCLV)[1-4] or the Itek Pockels readout optical modulator (PROM).[5]

Optical A/D conversion has been achieved for single-point inputs by electro-optical methods[6] in real time. Other techniques of nonlinear optical processing have performed A/D conversions by halftoning methods, although not in real time.[7-10]

The LCLV, PROM, and many other real-time optical input transducers rely on electro-optically controlled birefringence to produce a spatially varying linear differential phase retardation along two axes of a crystal. For this work a LCLV has been constructed with uniform perpendicular alignment of the liquid-crystal material so the device exhibits a pure birefringent effect that varies with local electric field. When the LCLV is placed between crossed polarizers, a sinusoidal variation of intensity transmittance with applied voltage is observed.[3-5] When a photoconductor is placed at the surface of the liquid-crystal cell, the local electric field is a function of the incident illumination.[1,2] The overall relationship between the intensity transmittance of the device and the incident intensity at any point is given ideally by the sinusoidal curve shown with dashes in Fig. 1(a).

The digital results of A/D conversion at each image point may be output serially as a bit sequence or in parallel as bit planes.[11] Bit planes are binary image planes, each of which displays the information of a

particular significant bit of the digitized image. The solid-line curves of Fig. 1 show the nonlinear transfer characteristic needed to produce the bit planes of the three-bit reflected binary or Gray code and their relationship to the dashed curves of sinusoidal device characteristics. When the output of Fig. 1(a) is thresholded at one half, a 1 output is produced above threshold and a 0 output below, as shown by the curves *with solid lines. This thresholding can be done elec-*tronically following light detection by a parallel array of sensors. The threshold output in Fig. 1(a) is the least significant bit of the three-bit Gray code. The other two bits are obtained by attenuating the input intensity effectively to rescale the horizontal axis. Use of the full dynamic range (0 to 8) gives the least significant bit. Attenuating the input by a factor of ½ (to the range 0
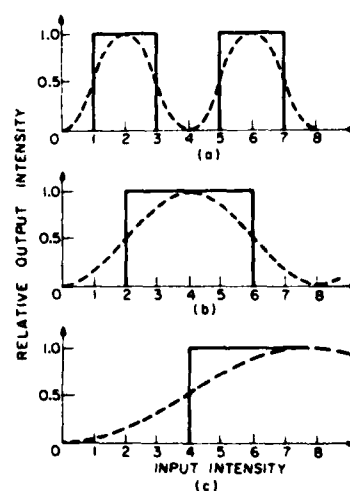

Fig. 1. Nonlinear characteristic curves required for the three-bit Gray code. Solid curves are the desired characteristics for the bit plane outputs. Dotted curves are the ideal sinusoidal responses of a linear birefringent device. Parts (a) through (c) represent increasingly significant output bits.
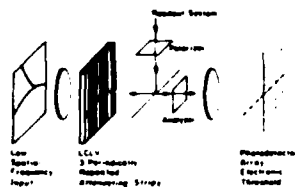
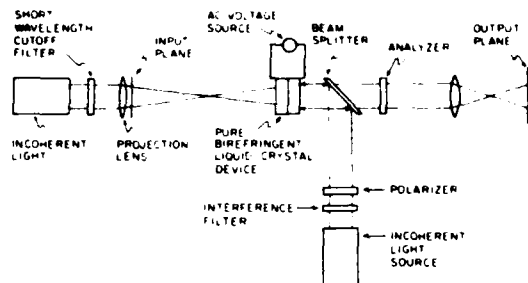Fig. 2.   System for parallel A/D conversion.

Fig. 3.   Experimental setup for real-time parallel analog-to-digital conversion.

to 4) gives the first cycle of the characteristic curve shown in Fig. 1(b). The last (most significant) bit is obtained by using an attenuation of one fourth so the curves of Fig. 1(c) result. Note that any continuous input between 0 and 8 gives a unique quantized three-bit output. Although the thresholded outputs in Fig. 1 are the three bits of the Gray code, other A/D code conversions, such as the usual straight binary code, can be achieved by translating these curves left or right along the horizontal axis. This can be done by introducing phase-retardation plates with different delays along orthogonal axes into the crossed polarizer system.

The system can produce these bits in parallel by placing an array of three periodically repeated attenuating strips over the write surface of the liquid-crystal device, as shown schematically in Fig. 2. The strips have attenuation factors of 1, $\frac{1}{2}$, and $\frac{1}{4}$, and the image of the strips is in register with a parallel photodetector array with electronic thresholding in the output plane. All three bits are sensed in parallel in this way. The period of the strips should be much smaller than the inverse of the maximum spatial frequency of the input picture to avoid aliasing. A two-dimensional array of attenuating spots with a corresponding detector array can also be used instead of the linear strip array. Simpler but slower operation can be achieved by using only one detector array and sequentially uniformly attenuating the entire input array. Ideas such as this have been used for electro-optic A/D conversion,[6] but none have used an optically controllable real-time device.

The experimental system shown in Fig. 3 was used to obtain the input–output characteristic of the pure birefringent LCLV and to demonstrate the concept. The incoherent source illuminating the input plane is a mercury-arc lamp. A fixed and rotatable polarizer pair in the input-light beam is used to vary the input-light intensity. The real-time device was a Hughes perpendicularly aligned nematic LCLV with a CdS photoconductor. The short-wavelength cutoff filter eliminates wavelengths shorter than 493 nm to make sure that the write-beam wavelength is matched to the sensitivity range of the CdS photoconductor. The read light source is a xenon-arc lamp. Because of the dispersion of birefringence in the liquid-crystal material, the read light should have a narrow spectral bandwidth. An interference filter with a peak wavelength of 434.7 nm and a bandwidth of 18.4 nm was used to meet this requirement for the read light. With no picture in the input plane, the output intensity varies in a quasi-sinusoidal fashion with increasing input illumination because of the changing birefringence. If the amount of birefringence varied linearly as a function of the write-beam intensity, a strictly sinusoidal variation of the output intensity would be expected. However, a number of factors, including the optical nature of the liquid crystal and the photoconductor characteristic properties, affect the output curve and produce an approximately sinusoidal output whose frequency varies (monotonically) with input intensity. The experimental response curve obtained is shown in Fig. 4.

Although the theory behind the A/D conversion assumes a strictly periodic response characteristic, it is possible to produce the desired bit planes by using the quasi-periodic response curves of the actual device. The trade-off is that nonuniform quantization results. The quantization levels obtained in this experiment are indicated in Fig. 4.

There are no attenuating strips on the liquid-crystal device used in this experiment. Instead, the bit planes were generated serially. Also, the output was recorded on hard-clipping film rather than a thresholding detector array. A test target was generated that consisted of an eight-gray-level step tablet. The gray levels were chosen to match the quantization levels shown in Fig. 4. This test object was imaged onto the liquid-crystal device, and the output was photographically hard clipped to produce the least significant bit plane of a three-bit A/D conversion. Next the write illumination intensity was decreased, effectively rescaling the response curve of the device to generate the next bit plane. The last bit plane (most significant bit) was obtained by attenuating the write intensity again and photographing the output. The input and the three-bit planes generated are shown in Fig. 5.
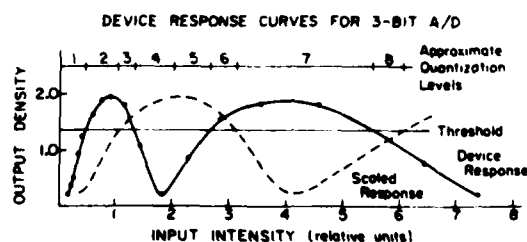

Fig. 4.   Response curve of the liquid-crystal device used for the three-bit A/D conversion. The solid curve is the measured response. The dotted curve represents the same response with a fixed attenuation of the input.
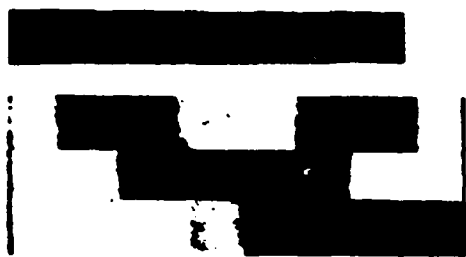
Fig. 5.   Direct analog-to-digital conversion. The eight-level analog input is shown at the top. Below is the binary-coded output in the form of three bit planes of the Gray code.

Although the output contains some noise, the experiment illustrates the principle of real-time parallel incoherent optical A/D conversion. It was found later that the computer-generated gray scale was somewhat noisy because of the grain of the high-contrast film used. It is possible that future experiments with cleaner inputs and improved periodic light valves could produce better experimental results and more bits of quantization.

The potential A/D conversion rate can be estimated from typical parameters of currently available devices. The important parameters are device resolution (typically 40 cycles/mm), device size (typically 50 mm × 50 mm), and speed (generally 30 frames per second). Multiplying all these parameters together and dividing by 3 for the attenuating strips implies an A/D conversion rate of 4×10^7 points per second. A fully parallel system with one light valve and detector array for each bit plane could achieve 1.2×10^8 points per second.

The feasibility of real-time parallel A/D conversion on two-dimensional inputs has been shown in this experiment. In contrast with other techniques of real-time nonlinear optical processing, such as halftoning,[12][14] the system operates with incoherent input. The requirements on the spatial and temporal coherence of the readout illumination are sufficiently relaxed that noise problems associated with coherent spatial filtering or transforming techniques are avoided. This technique also minimizes the spatial-frequency requirements of the real-time device because the sharp edges of the binary dots in halftoning do not have to be maintained.

Although these initial results are encouraging, further application of the technique must await improved real-time devices. The aperiodic nature of the LCLV results in unequal quantization intervals and limits the number of bits. The LCLV device used in this experiment is inherently aperiodic because of the nonlinear response of the photoconductor and the nonlinear relationship between applied voltage and effective bire-fringence. By altering the real-time device itself, the response may be improved somewhat. The possibility of making real-time devices (with liquid-crystal or PROM technologies) having a periodic response is being investigated.

References

1. T. D. Beard, W. P. Bleha, and S-Y. Wong, "AC liquid/crystal light valve," Appl. Phys. Lett. 22, 90 (1974).
2. J. Grinberg et al., "A new real-time non-coherent to coherent light image converter," Opt. Eng. 14, 217 (1975).
3. A. Armand, D. Boswell, A. A. Sawchuk, B. H. Soffer, and T. C. Strand, "Real-time nonlinear optical processing with liquid crystal devices," in Proceedings of the IEEE 1978 International Optical Computing Conference (Institute of Electrical and Electronics Engineers, New York, 1978), pp. 153-158.
4. A. Armand, D. Boswell, A. A. Sawchuk, B. H. Soffer, and T. C. Strand, "Approaches to nonlinear optical processing in real-time," in Proceedings of the International Commission for Optics Congress (Instituto di Optica, Madrid, 1978), pp. 253-256.
5. S. Iwasa and J. Feinleib, "The PROM device in optical processing systems," Opt. Eng. 13, 235 (1974).
6. H. F. Taylor, "An electrooptic analog-to-digital converter," Proc. IEEE 16, 1524 (1975).
7. A. W. Lohmann and T. C. Strand, "Analog-to-digital conversion of pictures with optical means," in Proceedings of Electro-Optics International Laser Conference (Industrial and Scientific Conference Management, Inc., Chicago, Ill., 1975), pp. 16-21.
8. T. C. Strand, "Non-monotonic nonlinear image processing using halftone techniques," Opt. Commun. 15, 60 (1975).
9. H. K. Liu, "Coherent optical analog-to-digital conversion using a single halftone photograph," Appl. Opt. 17, 2181 (1978).
10. H. K. Liu, "New and direct optical analog-to-digital conversion method," Opt. Lett. 3, 244 (1978).
11. W. K. Pratt, Digital Image Processing (Wiley-Interscience, New York, 1978), Chap. 12.
12. H. Kato and J. W. Goodman, "Nonlinear filtering in coherent optical systems through halftone screen processes," Appl. Opt. 14, 1813 (1975).
13. S. R. Dashiell and A. A. Sawchuk, "Nonlinear optical processing: analysis and synthesis," Appl. Opt. 16, 1009 (1977).
14. J. W. Goodman, "Operations achievable with coherent optical information processing systems," Proc. IEEE 65, 29 (1977).

1.4 Liquid Crystal Device Theory

In this program, a detailed theoretical analysis of liquid crystal light valves has been developed. Models have been developed for uniform perpendicular and for parallel aligned liquid crystal cell configurations and for the twisted nematic cell. Besides deriving expressions for transmission as a function of voltage in electrically controlled cells, photo-activated light valves have also been analyzed. The theoretical work has been complemented by experimental measurements of LCLV characteristics for various LCLV types. These measurements have substantiated the theoretical analysis. This work is the first comprehensive treatment of LCLVs with specific regard to those characteristics important to nonlinear processing applications. The results are described in detail in the Ph.D. thesis of J. Michaelson, which has been published as IPI Report 930 [46]. The paper, "A First Order Model of a Photo-Activated Liquid Crystal Light Valve," from the SPIE Los Angeles Technical Symposium in February 1980 [38] is reprinted here as a summary of these results.

A first-order model of a photo-activated liquid crystal light valve

J. D. Michaelson

The Aerospace Corporation, P.O. Box 92957, Los Angeles, California 90009
Department of Electrical Engineering, Image Processing Institute
University of Southern California, Los Angeles, California 90007

Abstract

A first order theoretical model of a thin nematic liquid crystal layer mated to a CdS/CdTe heterojunction photosensor is presented. Uniform parallel alignment of the liquid crystal molecules with the light valve substrates is assumed. The response of the liquid crystals is predicted through minimization of the distortion free energy density and the operation of the photosensor is obtained by assuming it to be a back biased light activated charge storage diode. Measurements of an actual liquid crystal light valve response are presented to verify the model.

Introduction

In order to effectively predict the performance of optical systems utilizing liquid crystal light valves (LCLV) as optical elements, it is necessary to obtain at least a first order model of the behavior of LCLVs under varying input intensity and bias voltage conditions. Past researchers have presented results describing the operation of the constituent parts of the LCLV as separate entities and it is the purpose of this paper to combine the associated theories to produce a usable model describing the operation of the complete LCLV.

The construction of a typical reflection mode photoactivated LCLV is shown in Fig. 1. In general the structure is divided into an input and output section by an opaque light blocking layer incorporated in the sandwich structure. The output section includes an internal dielectric mirror so that the read illumination (the light source to be controlled) passes through the liquid crystal layer, is reflected off the dielectric mirror, and again passes back through the liquid crystal cell before emerging from the device. The control or write illumination enters the input section of the device and impinges on the photosensitive layer. The photosensitive layer responds to intensity variations in the write illumination by switching the voltage applied across the device onto the liquid crystal layer. In this manner, optical control of the output illumination is achieved in the photoactivated liquid crystal light valve.

The two primary theories to be developed and then combined to form an overall LCLV model are: 1) the photosensor response as a function of applied intensity and bias voltage, and 2) the optical phase retardation represented by the liquid crystal layer as a function of applied cell voltage. The interaction of the liquid crystal layer and the photosensor must also be determined to produce the overall LCLV model. In particular the load impedance that the liquid crystal layer presents to the photosensor must be determined.

CdS/CdTe photosensor

In the most general terms, the photosensor acts as a light dependent impedance which locally switches the applied bias voltage onto the liquid crystal cell as a function of input light intensity. The operation of the CdS/CdTe heterojunction photosensor to be considered here is significantly more complex than a simple impedance change as a function of light intensity. The amount of bias voltage switched onto the liquid crystal layer depends not only on the light intensity but also on bias voltage amplitude and frequency, photosensor temperature, and load impedance. While a precise description of the photosensor operation has not yet been formulated and is beyond the scope of this paper to attempt, a number of simplifying assumptions may be made to obtain at least a first order approximation of the actual photosensor response. Experimental verification has shown these approximations sufficiently accurate to obtain reasonable predictions of light valve behavior under varying input intensity and bias voltage conditions [1,2].

A simplified equivalent circuit for the photoactivated light valve is shown in Fig. 2. From the figure, Z_{PC} is the impedance represented by the photosensor layer, Z_M is the series impedance of the dielectric mirror and inert insulating layers, and Z_{LC} is the impedance of the liquid crystal cell. If V_{LC} is the rms value of the applied bias

voltage, then from the figure the voltage V_{LC} developed across the liquid crystal cell is given by

$$V_{LC} = \frac{Z_{LC}V_S}{Z_T + Z_{LC}}$$

(1)

where Z_T is simply the sum of the impedances Z_{PS} and Z_M. The impedance Z_{LC} is in general a function of V_{LC}. The impedance Z_M may be represented by a pure capacitance as the mirror and insulating layers are simply stacked dielectric films. The impedance is readily calculated from the dielectric constants and known thicknesses of each of the layers. The impedance of any layer is given by

$$Z = \frac{1}{\jmath C}$$

(2)

where ω is the frequency of V_S in radians per second and C is the capacitance of the thin film.

The impedance Z_{PS} of the photosensor is somewhat more complicated and the model to be developed is that of Fraas et al [1,2] for a CdS/CdTe heterojunction photosensor. Z_{PS} represents the impedance of the charge storage diode shown in the simplified diagram of Fig. 2. If Q represents the total charge on the diode, then the characteristic Q vs. V curves for the structure are represented by [1,2]

$$V = \frac{Q^2}{2\epsilon\bar{n}} \qquad Q \le Q_\delta$$

(3)

$$V = \frac{\bar{n}\delta^2}{2\epsilon} + \frac{(Q-\bar{n}\delta)D}{\epsilon} \qquad Q \ge Q_\delta$$

(4)

where V is the instantaneous back bias voltage across the diode, ϵ is the CdS dielectric constant, D is the thickness of the CdS layer, and δ is the thickness of the high shallow trap density, high absorptive CdS region. The parameter $\bar{n}$ is the light intensity dependent electron population density in the high absorptive δ region and for low light levels is given by

$$\bar{n} = K\sqrt{I}$$

(5)

where I is the incident light intensity and K is a sensitivity coefficient whose value depends on temperature, frequency, and the physical constants of the CdS film. The threshold parameter Q_δ is the total charge in donor states and is given by

$$Q_\delta = \bar{n}\delta$$

(6)

The model described by Eqs. (3)-(6) assumes that all of the incident light is absorbed in the highly absorptive δ region. This assumption is reasonable for first order approximations but does lead to slight discontinuities in photosensor response predictions. Using Eqs. (3) and (4), representative Q vs. V curves for a 16 micron thick CdS layer are shown in Fig. 3 as a function of $\bar{n}$.

For a sinusoidally varying input bias voltage, if $2V_P$ equals the maximum inverse voltage across the diode, then the instantaneous back bias voltage will be given by

$$V = V_P(1+\cos\omega t)$$

(7)

The threshold voltage governing selection of either Eq. (3) or Eq. (4) is given by setting $Q=Q_\delta$ in either equation. Thus from Eq. (3)

$$V_T = \frac{Q_\delta^2}{2\epsilon\bar{n}} = \frac{\bar{n}\delta^2}{2\epsilon}$$

(8)

For $V \le V_T$, the instantaneous current in the photosensor is given by

$$i_1 = \frac{dQ}{dt} = -\omega\sqrt{\epsilon\bar{n}V_P} \; \sin\frac{\omega t}{2}$$

(9)

For $V \ge V_T$, then from Eq. (4)

$$i_2 = \frac{dQ}{dt} = \frac{-\omega\epsilon V_P}{D} \; \sin\omega t$$

(10)

The rms current I through the photosensor is given by

$$I^2 = \frac{1}{T} \int_0^T i^2 dt \tag{11}$$

where T is the period of one cycle, i.e., $T = 2\pi/\omega$. Now if $2V_P \leq V_T$, then Eq. (9) alone specifies the instantaneous current. Thus the rms current is given by

$$I_1 = \omega \sqrt{\frac{\varepsilon \bar{n} V_P}{2}} \tag{12}$$

If $2V_P > V_T$ the situation is somewhat more complicated with the instantaneous current being given by Eq. (9) for $V \leq V_T$ and then by Eq. (10) for $V > V_T$. The calculated current becomes

$$I_2 = \frac{\omega \varepsilon V_P}{D\sqrt{2\pi}} \left\{ \cos^{-1}\beta - \beta(1-\beta^2)^{1/2} + \frac{\bar{n}D^2}{\varepsilon V_P}\left[\pi - \cos^{-1}\beta + (1-\beta^2)^{1/2}\right] \right\}^{1/2} \tag{13}$$

where $\beta = \frac{\bar{n}\delta^2}{2\varepsilon V_P} - 1$. Equations (12) and (13) then relate the rms photosensor current to the incident light intensity and back bias photosensor voltage. Figure 4 shows a typical plot of I/ω vs. photosensor voltage. The combination of this data and the liquid crystal cell impedance data to be determined will uniquely relate the bias voltage and incident intensity to the voltage across the liquid crystal layer.

Liquid crystal cell

The best first order predictions of the behavior of nematic liquid crystals has been through the use of a continuum theory developed by Cseen [3], Zocker [4], and Frank [5]. The basis of the theory is the minimization of the free energy in the liquid crystal layer while under the influence of an applied external field. The distortion free energy density of the liquid crystals is given by

$$F = \frac{1}{2}\left[K_{11}(\operatorname{div} \bar{n})^2 + K_{22}(\bar{n}\cdot\operatorname{curl} \bar{n} + \bar{q}_0)^2 + K_{33}(\bar{n} \times \operatorname{curl} \bar{n})^2\right] \tag{14}$$

where $\bar{n}$ is the unit vector parallel to the local molecular axis, $\bar{q}_0$ is the periodicity of molecular rotation in the liquid crystal layer ($\bar{q}_0 = 0$ for a nematic system), and the K_{ii} are the Frank elastic constants for the liquid crystal material. The three terms in Eq. (14) correspond to the distortions of splay, twist, and bend shown diagrammatically in Fig. 5. When an external field is applied to the liquid crystal layer, a fourth term must be added to the free energy equation. This term is given by

$$F_E = -\frac{1}{2} \varepsilon_a(\bar{n}\cdot\bar{E})^2 \tag{15}$$

where $\bar{E}$ is the applied electric field vector and $\varepsilon_a = \varepsilon_{\parallel} - \varepsilon_{\perp}$ is the dielectric anisotropy.

When the liquid crystal molecular axis lies parallel with the substrate surfaces, minimization of the free energy equation leads to a closed form solution. The geometry is shown in Fig. 6. Taking note of the symmetry of the structure, the free energy is minimized by satisfying

$$\xi^2 \frac{d^2\phi}{dz^2} = \frac{\sin 2\phi}{2} \tag{16}$$

where

$$\xi = \left(\frac{K}{\varepsilon_a}\right)^{1/2} E^{-1} \tag{17}$$

Through further integration and application of boundary conditions, Eq. (16) becomes

$$\phi = 2\tan^{-1} e^{-z/\xi} \tag{18}$$

The total phase retardation through the cell of thickness d is given by

$$\delta = \frac{4\pi\Delta n}{\lambda} \int_0^{d/2} \sin^2\phi(z)dz \tag{19}$$

where d(z) is as given by Eq. (18).   Defining

$$\delta_0 = \frac{2\pi \Delta n d}{\lambda} \tag{20}$$

then eq. (19) becomes

$$\delta/\delta_0 = \frac{2\xi}{d} \tanh \frac{d}{2\xi} \tag{21}$$

With V=Ed, $V_C = 2(\frac{K}{\epsilon_a})^{1/2}$ and the aid of Eq. (17), Eq. (21) becomes

$$\delta/\delta_0 = \frac{V_C}{V} \tanh \frac{V}{V_C} \tag{22}$$

The normalized phase retardation vs. V_C/V is shown in Fig. 7. As seen in the figure,
for $V_C/V \ll 1$ the normalized phase retardation simply goes as $1/V$.

Liquid crystal cell impedance

As is the case for the phase retardation, the cell impedance for the parallel aligned
uniform cell has a closed form solution. From the geometry shown in Fig. 6, it is seen
that the effective dielectric constant is given by

$$\epsilon_e = \epsilon_{||} \cos^2\phi + \epsilon_\perp \sin^2\phi \tag{23}$$

From Eq. (18)

$$\cos^2\phi = \tanh^2(z/\xi) \tag{24}$$

and from Eq. (23), we obtain

$$\epsilon_e = \epsilon_\perp + (\epsilon_{||} - \epsilon_\perp)\cos^2\phi \tag{25}$$

Combining Eqs. (24) and (25), then

$$\epsilon_e = \epsilon_\perp + (\epsilon_{||} - \epsilon_\perp)\tanh^2(z/\xi) \tag{26}$$

Thus the capacitance of any layer at position Z in the cell is given by

$$C(z) = \frac{\epsilon_0 \epsilon_e(z) A}{dz} \tag{27}$$

Integrating over the length of the cell, the total normalized cell capacitance is given by

$$C_T/A = \frac{\epsilon_0}{d/\epsilon_{||} \left\{ 1 + \frac{V_C}{V} \sqrt{\frac{\epsilon_{||} - \epsilon_\perp}{\epsilon}} \tan^{-1}\left[\sqrt{\frac{\epsilon_{||} - \epsilon_\perp}{\epsilon}} \tanh \frac{V}{V_C} \right] \right\}} \tag{28}$$

For $\epsilon_{||} = 16$ and $\epsilon_\perp = 5$, Fig. 8 shows the cell capacitance per unit area vs. normalized
voltage for an 11 micron thick parallel aligned cell.

The results of the preceding three sections may now be used to predict the LCLV
response to variations in both input light intensity and applied bias voltage. For a
given set of device parameters, Eqs. (12), (13), and (28) can be simultaneously solved to
provide the voltage appearing across the liquid crystal cell for any set of bias voltage
and input light intensity conditions. Equation (22) can then be used to determine the
phase retardation of the liquid crystal cell for the given conditions. If the device is
operated between a crossed polarizer/analyzer as shown in Fig. 9, then the output
intensity is related to the phase retardation by

$$I_{OUT} = I_0 \sin^2\delta \tag{29}$$

where I_0 is the magnitude of the incident read light intensity.

Experimental Results

To verify the validity of the above model, measurements were made on a parallel aligned
LCLV.   The device was constructed with a broad band internal dielectric mirror and an 11
micron thick CdS/CdTe photosensor. The thickness of the liquid crystal layer was known to
be between 2 and 3 microns. Using the test configuration shown in Fig. 9, i.e. a crossed
polarizer/analyzer pair oriented at 45 degrees to the liquid crystal axis, a read

illumination of wavelength 632.8 nm, and a write illumination of wavelength 514.5 nm, then Fig. 10 shows the transmission characteristics of the cell as a function of applied bias voltage. The write illumination was set at its maximum value (approximately 2.8 mw/cm²) in order to maximize the amount of bias voltage switched to the liquid crystal layer and thus obtain the largest possible phase retardation change over the range of bias used. At zero volts bias, the parallel aligned cell will exhibit its maximum phase retardation δ_0. Thus from Eq. (29) relating the intensity transmission to the phase retardation for a reflection mode device and the zero bias voltage data of Fig. 10, δ_0 is given by

$$\delta_0 = \sin^{-1}(\frac{I_{OUT}}{I_0})^{1/2} = n\pi \pm .851 \quad \text{radians} \tag{30}$$

To determine the absolute magnitude of δ_0, Eq. (20) together with the known dimensional range of the liquid crystal thickness (2-3 microns) implies $4.96 \leq \delta_0 \leq 7.45$. Thus the factor n in Eq. (30) is determined to be 2. To determine the proper quadrant for δ_0, from Fig. 10 it is noted that as the bias voltage is increased from zero volts the device transmission increases reaching a maximum at approximately 6.7 volts bias. From Eq. (29), relative transmission maximas occur at integer multiples of $\pi/2$ radians of phase retardation. This observation together with the fact that the phase retardation decreases with increasing cell voltage for a parallel cell clearly necessitates the use of the negative sign in Eq. (30) giving a value for δ_0 of 5.4324 radians. Using this value in Eq. (29), the actual cell thickness is calculated to be 2.188 microns.

Using the value for δ_0 determined above and the data of Fig. 10, the normalized phase retardation vs. inverse normalized voltage is shown in Fig. 11 together with the theoretical curve of Fig. 7. Agreement of the data with the theory in the figure is reasonable. The deviations may be attributed to a combination of measurement error, second order effects making the relationship of the bias voltage to the cell voltage nonlinear, and the deterioration of the theoretical model for voltages near the critical voltage threshold.

To determine the theoretical response of the device to changes in input intensity under fixed bias conditions, it is first necessary to determine the impedance of the internal dielectric mirror. The mirror impedance is in series with the impedance represented by the liquid crystal layer and the light-dependent impedance of the CdS/CdTe photosensor. Thus for a given photosensor current, a fraction of the bias voltage will be present across the photoconductor, a second fraction across the mirror, and the remainder will be present across the liquid crystal layer. The mirror was designed to be broadband and consisted alternately of 8 layers of MgF and 7 layers of ZnS. From the known thicknesses of the individual layers, the total mirror capacitance was calculated to be 2534 pf/cm².

For a photosensor thickness of 11 microns, $\epsilon = 4.4275 \times 10^{-11}$, $\delta = 2.6667$ microns, a mirror capacitance of 2534 pf/cm², a liquid crystal capacitance of 2024 pf/cm² as calculated for a thickness of 2.188 microns, and a bias voltage of 12.37 volts, then using the photosensor theory developed previously, Fig. 12 shows the calculated liquid crystal voltage as a function of input intensity in db. If this data is then applied to the theoretical retardation vs. cell voltage given by Eq. (22), then for a maximum retardation of 5.4324 radians and a critical voltage of 2.47 volts, the solid line in Fig. 13 shows the calculated device transmission as a function of db input intensity. Plotted together with the theoretical curve is actual data taken from the experimental device for a bias voltage of 12.37 volts. The data is seen to be in good agreement with theory thus demonstrating the validity of the theoretical models.

Summary

A model has been developed for predicting the response of liquid crystal light valves to variations in input light intensity and bias voltage. The model assumed a thin nematic liquid crystal layer with parallel alignment of the molecules with the device substrates. The light valve photosensor was assumed to be a reverse biased CdS/CdTe heterojunction. The overall light valve response to changes in both input light intensity and bias voltage was predicted by first calculating the steady state rms current through the photosensor/liquid crystal sandwich structure as a function of input conditions. The field across the liquid crystal layer was then related to the rms current and through calculated phase retardation vs. field the optical response of the device between a crossed polarizer/analyzer was determined. Experimental results were shown for a reflection mode device and demonstrated reasonable agreement with the predicted response.

References

1. L.M. Fraas, et al., "Novel Charge-Storage-Diode Structure for use with Light Activated Displays," Journal of Applied Physics, Vol. 47, No. 2, pp. 576-583, February 1976.

2. L.M. Fraas, et al., "AC Photoresponse of a Large Area Imaging CdS/CdTe Heterojunction," Journal of Applied Physics, Vol. 47, No. 2, pp. 584-590, February 1976.

3. C. Cseen, Transactions Faraday Society, Vol. 29, page 883, 1933.

4. H. Zocher, Transactions Faraday Society, Vol. 29, page 945, 1933.

5. F. Frank, Discussions Faraday Society, Vol. 25, pp. 19-28, 1958.
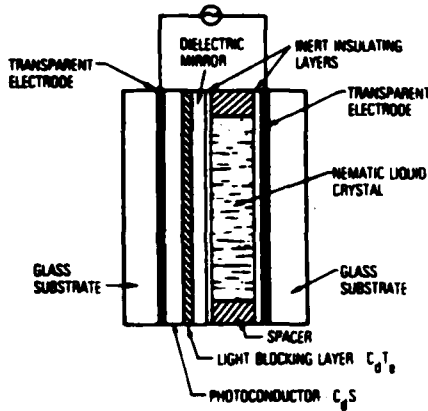
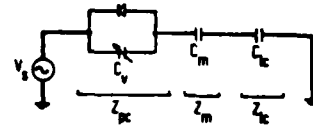

Figure 1.   Cross section of photo-activated light valve.
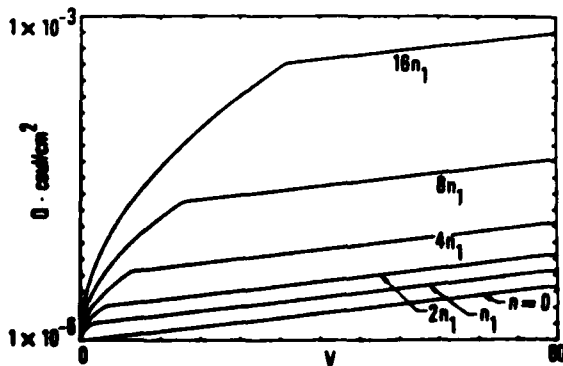

Figure 2.   Simplified equivalent circuit of LCLV.

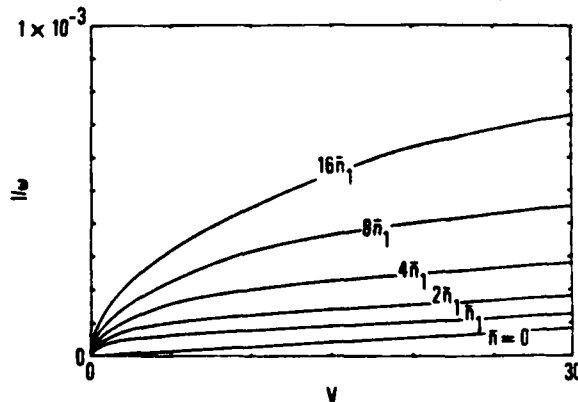Figure 3.   Q vs. V curves for CdS/CdTe photosensor.

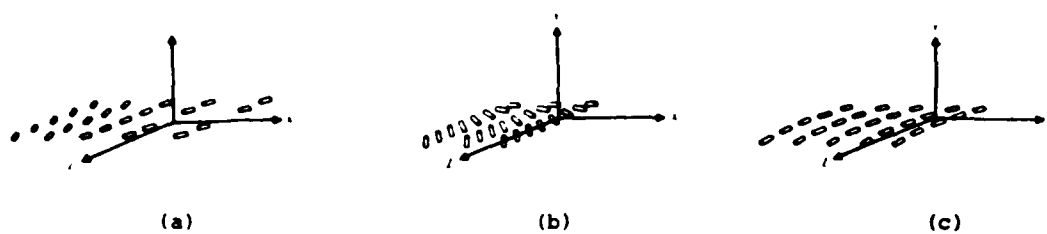Figure 4.   Normalized photosensor current vs. applied voltage.

Figure 5.   Liquid crystal molecular distortions.
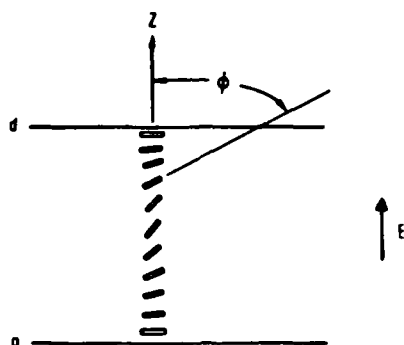a) Splay, b) Twist, c) Bend.

Figure 6.   Geometry of uniform parallel cell.
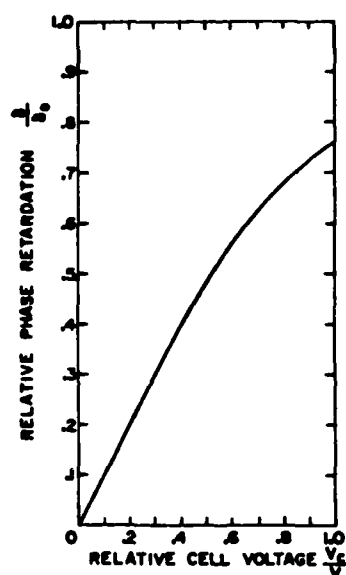
Figure 7. Normalized phase retardation vs.
inverse normalized voltage.

Figure 8.   Cell capacitance vs. normalized
voltage.

Figure 9.   Test configuration for measuring
response of LCLV.

Figure 10.   Measured transmission vs. bias
              voltage.

Figure 11.   Measured phase retardation vs.
              inverse voltage.
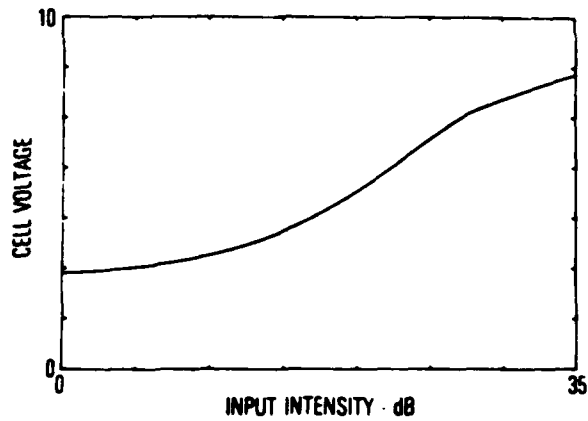
Figure 12.   Calculated cell voltage vs.
              input intensity.
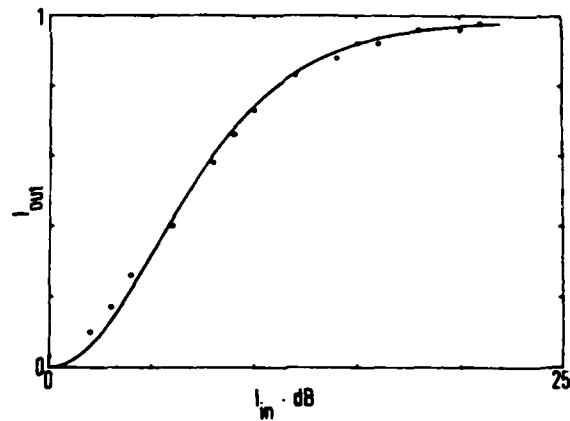
Figure 13.   Measured and calculated
              response of LCLV.

1.5 Multiple Light Valve System

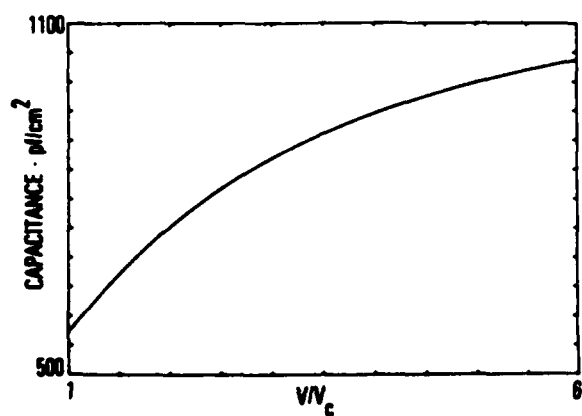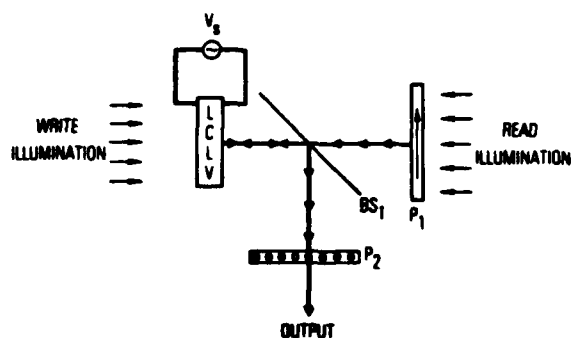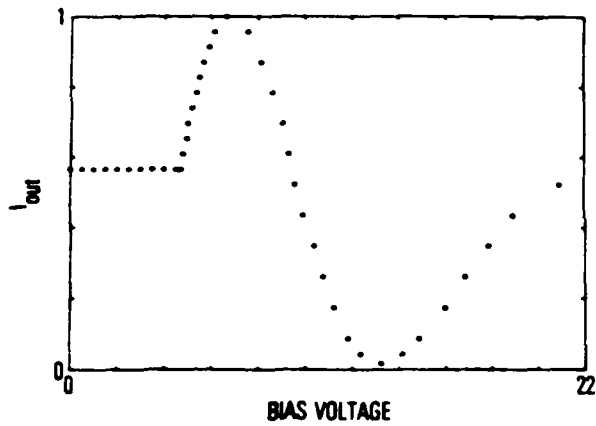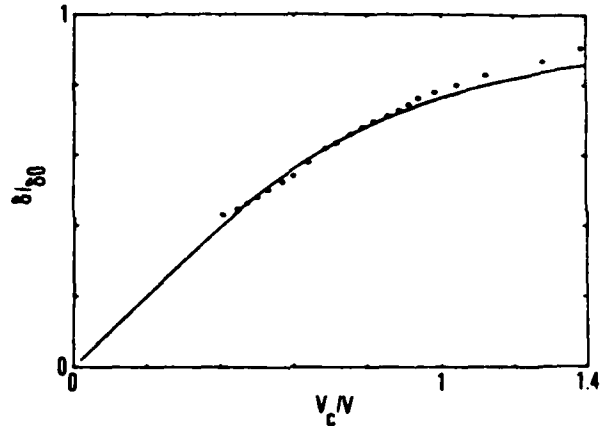The result of the theoretical and experimental work on liquid crystal devices described in Section 1.4 have been utilized in the development of a generalized nonlinear image processing which is referred to as the multiple light valve system (MLVS). The principle of this system is to implement a time varying level slice coupled with a synchronous electronically programmed gain to produce an arbitrary nonlinearity. In the past year new experimental results have been obtained with this system. In particular a three-bit A/D conversion has been demonstrated as well as a variable level slice. The results are described in detail in the Ph.D. thesis of J. Michaelson, which has been published as IPI Report 930 [46]. The paper, "Nonlinear Optical Processing Using Liquid Crystal Light Valves," from the SPIE Los Angeles Technical Symposium in February 1980 [39] is reprinted here as a summary of these results.

Nonlinear optical processing using liquid crystal light valves

J. D. Michaelson*, A. A. Sawchuk

Department of Electrical Engineering. Image Processing Institute
University of Southern California, Los Angeles, California 90007

Abstract

A method is presented to realize real time nonlinear operations on two dimensional images through the use of multiple liquid crystal light valves. The technique allows the use of either coherent or incoherent illumination and provides for real time control and alteration of the specific nonlinear operation being performed. Experimental results are given for level slice, logarithm, exponentiation, and A/D conversion.

Introduction

In recent years a number of methods have been described for realizing nonlinear optical transformations on two dimensional input images. The various methods include the use of saturable absorbers [1], coherent optical feedback [2], hybrid optical-electronic systems [3,4], and halftone screen processing [5-8]. More recent innovations have taken advantage of the unique characteristics of optical elements to directly obtain specific nonlinear transformations. In particular, the liquid crystal light valve has been used for the specific operation of parallel analog-to-digital conversion of input images [9]. In general the above implementations suffer from one or more disadvantages. They either require large amounts of optical power as with saturable absorbers, do not offer versatility in the types of transformations that may be performed, require critical optical alignment, or do not offer real time operation. It is the purpose of this paper to describe a system which is not only capable of real time operation but also provides versatility in the number and types of operations which can be performed. As will be shown, the system takes advantage of the polarization properties of liquid crystal light valves to achieve the nonlinear operations.

Generalized nonlinear transformation system

The nonlinear transformation system described here essentially performs a mapping of the intensity variations of a two dimensional input image into two dimensional constant magnitude but temporally separated light impulses. This constitutes a scanned level slice operation. The constant magnitude impulses are then weighted as a function of time with a temporal weighting function formulated to give the desired nonlinear transformation. The weighted impulses are then integrated over an appropriate time interval resulting in a two dimensional nonlinear transformed output image. The operation is shown schematically in Fig. 1 for a simple three intensity level, two dimensional input image. The intensity to time converter maps input intensities over the range of 0 to I_{MAX} into the time interval [0,T]. Thus for a linear mapping the output plane for the intensity to time converter will remain dark during the time interval $0<t<t_1$ since there exists no intensity components in the input image with values between $I=0$ and $I=I_1$. At time t_1 corresponding to the input intensity I_1, the output plane will have a constant intensity response over all portions of the plane corresponding to that part of the input image for which $I=I_1$. Similar output responses occur at times t_2 and t_3 as shown in the figure. For all other times $0<t<T$; $t \neq t_1,t_2,t_3$ the output intensity remains at zero. Representing the idealized light impulses by the Dirac delta function $\delta(x,y,t)$, then at the output plane of the intensity-to-time converter the intensity distribution is given by

$$I_T(x,y,t) = I_{MAX}\delta(t - \frac{I(x,y)}{I_{MAX}} T) \tag{1}$$

where $0 \leq t \leq T$ and $0 \leq I(x,y) \leq I_{MAX}$.

Referring again to Fig. 1, the temporal intensity weighter is simply an electrooptic attenuator which weights the constant intensity, time sequential impulses emerging from the intensity-to-time converter in the desired nonlinear manner. The nonlinearity is

---

*J.D. Michaelson is also with the Aerospace Corporation, P.O. Box 92957, Los Angeles, Ca. 90009.

introduced by applying a nonlinearly shaped voltage waveform to the temporal intensity weighter during the time interval [0,T]. Thus if f(t) represents the desired time dependent nonlinear attenuation function present in the intensity weighter during the interval [0,T], then the intensity distribution at the output of the weighter is given by

$$I_W(x,y,t) = f(t)I_T(x,y,t) \; . \tag{2}$$

The final operation depicted in Fig. 1 is that performed by the temporal integrator. The time sequential weighted impulses $I_W(x,y,t)$ are summed over the time interval [0,T] thus removing the time dependence. The result is that at time t=T a nonlinearly transformed input image will be present at the output of the integrator, i.e.,

$$I_0(x,y) = \int_0^T f(t)I_{MAX}\delta(t - \frac{I(x,y)}{I_{MAX}}T)dt \tag{3}$$

$$I_0(x,y) = I_{MAX}f\left[\frac{I(x,y)T}{I_{MAX}}\right] \; . \tag{4}$$

Equation (4) defines the system transfer function. Thus for the simple case of

$$f(t) = \frac{t}{T} \tag{5}$$

then

$$I_0(x,y) = I_{MAX}\left[\frac{I(x,y)}{I_{MAX}}\right] = I(x,y) \tag{6}$$

which is simply a one-to-one linear transformation from input to output. It should be noted that one of the key features of this type of system is the ability to arbitrarily and in real time change the form of the nonlinear transformation. The nonlinearity introduced through f(t) above is in general related to the voltage applied to the temporal intensity weighter by the attenuation transfer function ϕ_A of the electrooptic attenuator, i.e.,

$$f(t) = \phi_A V(t) \; . \tag{7}$$

As will be shown in the following section, a real time implementation of this system using multiple liquid crystal light valves provides for real time control of v(t) via a microprocessor or minicomputer.

Liquid crystal implementation

The ideal nonlinear processing system described in the previous section can be approximated using the polarizing properties of liquid crystal light valves. To demonstrate this, the system will be divided into four distinct functional areas, three of which are implemented with liquid crystal light valves. The functions to be considered are 1) an intensity notch function, 2) a contrast inverter/threshold operation, 3) an intensity weighter, and 4) the integration function. The first two of these functions comprise the intensity-to-time converter. Together they perform the mapping of the input intensity variations into the time sequential constant amplitude light impulses. For reasons that will become apparent, the operation is implemented by mapping the two dimensional input variations into time sequential intensity notches (function one), and then contrast inverting the notch responses to obtain time sequential intensity level slices (function two). Functions three and four directly implement the temporal weighter and integration operations described in the previous section.

Intensity notch function

To demonstrate implementation of the notch function using light valves, consider the reflection mode light valve system shown in Fig. 2. The read illumination enters from the right where it is polarized by polarizer P_1. The angle of polarization is set such that it subtends an angle of 45 degrees to the liquid crystal molecular axis. The light passes through P_1 directly through beam splitter BS_1 and enters the light valve structure. The light then passes through the liquid crystal layer, is reflected from the internal dielectric mirror in the device and passes again through the liquid crystal layer before emerging toward BS_1. As the light traverses the liquid crystal layer, the two components of the incident light in the X and Y directions undergo a differential phase change determined by the phase retardation of the liquid crystal cell. From the light valve, the

light is then reflected off of beamsplitter BS_1 where it then passes through polarization analyzer P_2 whose polarization angle is set at 90 degrees to polarizer P_1. The resultant intensity of the light emerging from P_2 is related to the phase retardation imposed by the liquid crystal device by

$$I_R = I_0 \sin^2 \delta \qquad (8)$$

where I_0 is the incident read light intensity and δ is the phase retardation.

Using calculated values of phase retardation vs. cell voltage and relationship (8), Fig. 3 shows the log intensity vs. cell voltage for a typical cell aligned as in Fig. 2. As shown in the figure, a sharp null occurs at a cell voltage of 4.09 volts. If the liquid crystal cell is mated to a photoconductor, the cell voltage then becomes a function both of the incident write intensity on the photoconductor and the bias voltage applied to the overall structure. For a given write intensity, the photoconductor will switch a fixed ratio of the bias voltage onto the liquid crystal layer. Thus if the bias voltage is swept over appropriate limits, the fraction of the bias voltage switched to the liquid crystal layer will become equal to the null voltage of Fig. 3 at some bias voltage V_1. This will result in minimal intensity transmission of the output read light. For any other input write intensity, a unique fraction of the bias voltage is transferred to the liquid crystal layer. Thus the critical null voltage of Fig. 3 will be reached at different points during the sweep of the bias voltage. If the bias voltage is swept linearly with time, this then establishes a one-to-one mapping of intensity notch with time.

To illustrate the process, consider a 2 micron perpendicularly aligned liquid crystal cell mated to a 16 micron thick CdS/CdTe photosensor. Using typical photosensor parameters [10,11], $\delta = 2.67$ microns, $\epsilon = 4.43 \times 10^{-11}$, then Fig. 4 shows the theoretical light valve response as a function of bias voltage for three input intensities separated by 3 db.

Contrast inverter

The intensity-to-time converter in the overall processing system requires constant magnitude light impulses as its output rather than the intensity nulls given by the intensity notch generator. Through contrast inversion the nulls obtained from the notch generator can be converted into the desired impulses or light peaks. Contrast inversion is easily implemented using the polarization properties of liquid crystal cells. The function is best implemented with the reflection mode twisted nematic type light valve with the polarizer/analyzer pair oriented in the same direction. It has been shown [12] that a cell with an overall molecular twist of 45 degrees provides the maximum on-off transmission ratio. For this reason the 45 degree twist cell was used to implement the contrast inversion.

The transmission vs. input intensity for a 4 micron, 45 degree twisted nematic LCLV placed between a polarizer and analyzer oriented in the same direction is shown in Fig. 5. In the figure, the ordinate is normalized intensity transmission for 514.5 nm read illumination. The abscissa is in relative db of input intensity. As seen in Fig. 5 the transfer function has the necessary slope to provide contrast inversion, i.e. smaller input intensity results in greater intensity transmission at the output of the device.

If one of the notch responses shown in Fig. 4 is used as the input to the above light valve, the effects of the contrast inversion can be seen in Fig. 6. To obtain the results shown in the figure, the input to the contrast inverter, while following on a db basis the transmission characteristic of the notch generator, was adjusted such that the -30 db point on the null curve corresponded to the -46 db input point on the contrast inverter transfer curve. Such scaling is readily accomplished in an actual system by adjusting the intensity of the read illumination to the notch generator. In the present discussion, this illumination modified by the transfer characteristics of the notch generator becomes the input write illumination to the contrast inverter. Figure 6 points out an added benefit of using the light valve for contrast inversion. Due to the limiting characteristics of the inverter transfer curve, the device also performs a thresholding operation on the input intensity response. Thus the relatively broad input null response results in a significantly more narrow output response as a function of notch generator bias sweep voltage. The output then more closely resembles the ideal delta function type response desired for the nonlinear processing system's intensity to time converter. Clearly, the more narrow the light impulses, the greater will be the resolution of the processing system.

Temporal weighter

The second major operation in the nonlinear processing system depicted in Fig. 1 is the

weighting of the light impulses emanating from the intensity-to-time converter by the temporal intensity weighter. As described previously, the temporal intensity weighter is the element in the processing system used to introduce the desired nonlinear operation on the system's input intensity distribution. The weighter is in effect an electrooptic attenuator with sufficient dynamic range to accomplish the desired nonlinear transformation.

A transmission type liquid crystal cell operating between a crossed polarizer/analyzer can conveniently be used for the electrooptic attenuator. To illustrate, consider a perpendicularly aligned uniform cell of thickness 8 microns. For a unit magnitude input intensity, Fig. 7 shows the transmission/attenuation characteristics of the cell as a function of applied voltage.

Temporal integrator

The final function in the nonlinear optical processor depicted in Fig. 1 is that of temporal integration. The nonlinearly weighted impulses emerging from the temporal weighter are distributed sequentially over the time interval [0,T] corresponding to the sweep period of the bias voltage on the intensity notch generator. The purpose of the integrator then is to accumulate the weighted light impulses over this time interval and present them in parallel form at the end of the sweep period. This effectively removes the time element from the processing operation.

Although some secondary storage effects in the liquid crystal light valves were observed during this study, the light valve is basically not a storage device and therefore cannot be used for the integration function. A number of devices do exist, however, that can suitably perform the integration. Two such devices used in this study are the silicon vidicon TV camera tube and photographic film. Using a vidicon, real time operation of the processing system is achievable. The manner in which the vidicon is used for the integration process is to halt the scanning on the vidicon surface during the bias sweep interval [0,T]. This allows the light from the temporal weighter to be accumulated and stored as a charge distribution on the photosensitive surface of the vidicon. At the end of the sweep period, the vidicon scan is resumed thus reading out the integrated charge for presentation on a suitable monitor or transmission over a communication link as desired.

The light integrating properties of photographic film are well known and offer a simple means of performing the integration task. While the use of photographic film precludes real time operation for many applications its use as the final integrator is tolerable and even desirable. This is particularly true if the nonlinear processor represents the final operation in a more complex image processing system where the final processed image is to be retained for observation or further analysis. A vidicon system was used extensively during this study to observe the operation of the processing system. However, the results presented in this paper were all obtained using photographic film as the temporal integration medium.

A third candidate for the temporal integration function is the class of optical and electrooptical devices capable of real time parallel image storage. Of particular interest is the PROM (Pockels Readout Optical Modulator) device [13]. While its use in the processing system was not investigated to any length during this study, it does offer significant potential as the final element in the nonlinear processor. The primary advantage of using such a memory device is that at the end of the integration period the final image is instantaneously available in coherent form for use in further optical processing operations. This is particularly advantageous if the nonlinear processor is simply one of several operations being performed on the original input image. A specific example of such an operation is in homomorphic image filtering.

Nonlinear Processing System

In the previous sections, methods for implementing each of the four basic functions of the nonlinear processor were described. Cascading each function as described, Fig. 8 shows one possible hardware configuration for realizing the overall processor. Lens L_1 images the input scene, image, or data onto the face of light valve $LCLV_1$. $LCLV_1$ is the notch generator described previously. Its bias voltage is derived from a programmable voltage source VS_1, that is controlled by a microprocessor system to produce the desired sweep voltage. The read illumination I_1 for $LCLV_1$ is polarized by P_1, passes through the light valve by reflection off of beamsplitter BS_1, and then is transmitted through BS_1 to the crossed analyzer P_2. From P_2 the light is focused by lens L_2 onto the contrast inverter implemented by light valve $LCLV_2$. The input intensity to $LCLV_2$ is appropriately scaled by adjusting the read illumination source I_1. The contrast inversion is completed as illumination I_2 passes through polarizer P_3, beamsplitter BS_2, the light valve $LCLV_2$, and finally out through parallel analyzer P_4. The fixed bias voltage for the contrast

inverter is supplied by voltage source VS_2. The polarized light from P_4 is imaged by the system of lenses L_3 and L_4 through the temporal weighter implemented with $LCLV_3$, crossed analyzer P_5, and finally onto the vidicon integrator. The bias voltage for temporal weighter $LCLV_3$ is derived from programmable source VS_3, and is controlled in conjunction with source VS_1 by the microprocessor control system. The microprocessor further controls the scan time of the vidicon integrator, providing a command at the appropriate time to scan the vidicon's photosensitive surface and send the processed image to the display unit.

Experimental Results

As shown in Fig. 8, the operation of the processing system was governed by a microprocessor-based controller. The controller performed the task of simultaneously providing the swept bias source for the intensity notch generator and the nonlinearly shaped bias source for the temporal weighter. When the vidicon camera system was employed for the final integration task, the microprocessor controller also supplied appropriately timed signals to inhibit or start the vidicon raster scan as described previously. The digitally based control system derived the two bias voltages through the use of D/A converters and a pair of four quadrant analog multipliers operating on a constant voltage AC source.

The transfer function of the intensity notch generator was carefully measured and the data reflecting the voltages at which intensity nulls occurred over an input intensity range of 26 db was stored in the microprocessor memory. Similarly, the voltage vs. attenuation characteristic of the temporal weighter was measured and the results stored in memory. Using this data base, the microprocessor was then programmed to perform four nonlinear operations upon command, i.e. level slice, logarithm, exponentiation, and A/D conversion.

Figures 9-12 show the preintegration responses of the processing system during a single sweep period of a level slice operation. A known constant intensity was input to the system during the sweep period. Figure 9 shows the response of the intensity notch generator as a function of sweep time. In Fig. 10, the intensity out of the contrast inverter/thresholder is shown for the same sweep interval. Figure 11 shows the voltage out of the D/A converter used to control the bias supply for the temporal weighter for the level slice operation. For the simple case of a level slice, the voltage limits correspond to the voltages necessary to switch the temporal weighter from maximum attenuation to maximum transmission. The final preintegration output intensity from the system is shown in Fig. 12.

Similar discrete intensity response measurements were made with the microprocessor placed in the logarithm and exponentiation modes. Repeated measurements of the output intensity were made in each mode as the input intensity was varied in 2 db steps over a total range of 20 db. The results for the logarithm and exponentiation operations are shown in Figs. 13 and 14 together with the appropriate calculated responses. The slight deviations of the measured values from the calculated curves are attributable not only to measurement error but also to the tendency of the light valves' transfer functions to change slightly with temperature.

The response of the system to operations on variable intensity, two dimensional input images is shown in Figs. 15 through 17. Figure 15 shows the original discrete intensity test image used as input to the system. The test pattern cells spanned a range of 23 db of input intensity with each cell being repeated a minimum of 3 times throughout the pattern. Figure 16 shows the integrated system response for a simple level slice operation on the test pattern.

The results of the slightly more complex operation of A/D conversion are shown in Fig. 17. The third row of the input intensity test pattern of Fig. 15 was digitized to 3 bits, each output image bit plane requiring a separate processor operation. The microprocessor was programmed to perform the digitization over db input intensity, i.e. eight distinct 3 db intensity bands spanning 24 db. The choice was somewhat arbitrary and through simple reprogramming of the microprocessor controller the digitization could be performed on the basis of absolute intensity.

The preceding results all were obtained using photographic film for the final integration process. As mentioned previously, the vidicon camera system was used extensively throughout the experimentation primarily to demonstrate the real time operating characteristics of the processing system. Using the vidicon system, real time operation could be demonstrated by translating the input image and observing the corresponding movement of the processed image on the camera monitor. The results obtained for stationary images using the vidicon system were nearly identical to those presented in this paper.

MICHAELSON, SAWCHUK

Summary

A multiple liquid crystal light valve system capable of performing real time nonlinear image transformations has been described. Experimental results for the specific nonlinear operations of level slice, logarithm, exponentiation, and A/D conversion were presented. It was shown that not only could input images be operated on in real time but also that the specific nonlinear operation could be altered in real time. Further, it was shown that the nature of the system allows for use of either coherent or incoherent light for the processing operation.

References

1. K.T. Stalker and S.H. Lee, "Use of Nonlinear Optical Elements in Optical Information Processing," J. Opt. Soc. Am., Vol. 64, page 545, 1974.
2. S.H. Lee, "Optical Processing with Nonlinearity and Feedback," Proceedings Electro-Optics/International Laser Conference 1975, Anaheim, California, pp. 22-30, 1975.
3. G. Hausler and A. Lohmann, "Hybrid Image Processing with Feedback," Optics Communications, Vol. 21, pp. 365-368, 1977.
4. A. Lohmann, "Suggestions for Hybrid Image Processing," Optics Communications, Vol. 22, pp. 165-168, 1977.
5. M. Marquet and J. Tsujiuchi, "Implementation of Particular Aspects of Dehalftoned Images," Optica Acta, Vol. 8, pp. 267-277, 1961.
6. H. Kato and J.W. Goodman, "Nonlinear Filtering in Coherent Optical Systems Through Halftone Screen Processes," Applied Optics, Vol. 14, pp.1813-1824, 1975.
7. S.R. Dashiell and A.A. Sawchuk, "Optical Synthesis of Nonlinear Nonmonotonic Functions," Optics Communications, Vol. 15, pp. 66-70, 1975.
8. T.C. Strand, "Techniques and Applications of Nonlinear Processing with Halftones," Proc. SPIE, 20th Annual Technical Symposium, San Diego, California, August 1976.
9. A. Armand, A.A. Sawchuk, and T.C. Strand, "Approaches to Nonlinear Optical Processing in Real Time," Proc. International Commission for Optics Congress, Madrid, Spain, September, 1978.
10. L.M. Fraas, et al., "Novel Charge-Storage-Diode Structure for use with Light Activated Displays," Journal of Applied Physics, Vol. 47, No. 2, pp. 576-583, February 1976.
11. L.M. Fraas, et al., "AC Photoresponse of a Large Area Imaging CdS/CdTe Heterojunction," Journal of Applied Physics, Vol. 47, No. 2, pp. 584-590, February 1976.
12. J. Grinberg, et al., "A New Real-Time Non-Coherent to Coherent Light Image Converter," Optical Engineering, Vol. 14, No. 3, pp. 217-225, 1975.
13 S. Iwasa and J. Feinleib, "The PROM Device in Optical Processing Systems," Optical Engineering, Vol. 13, pp. 235-242, 1974.
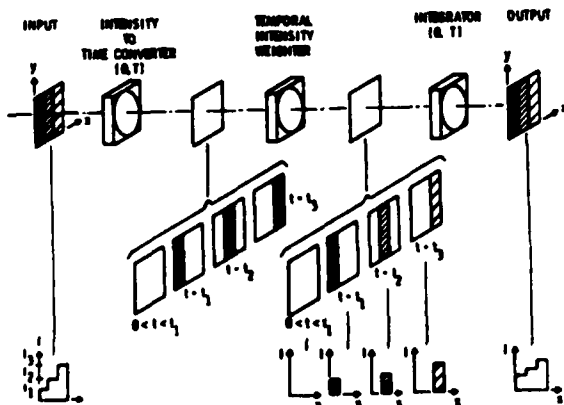
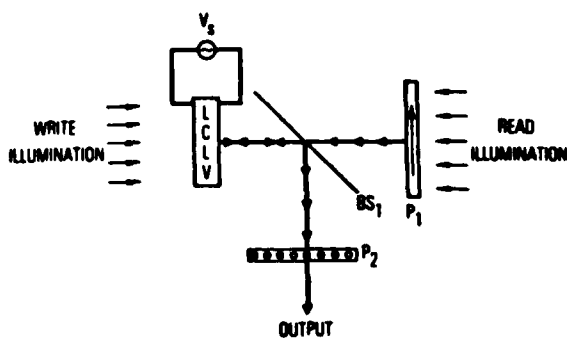Figure 1. Operation of nonlinear image processor

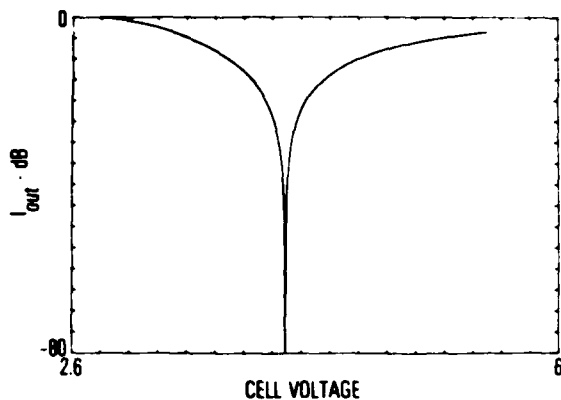Figure 2. Intensity notch generating subsystem

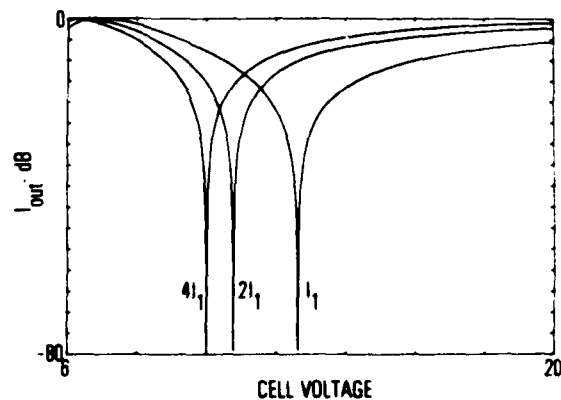Figure 3. Notch generator output intensity vs. cell voltage

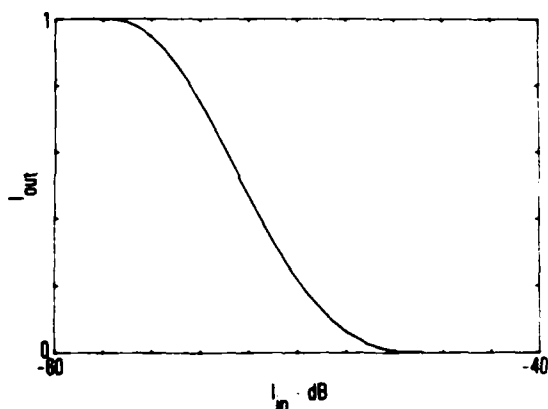Figure 4. Notch generator response for three separate input intensities

Figure 5. Intensity transfer function of contrast inverter
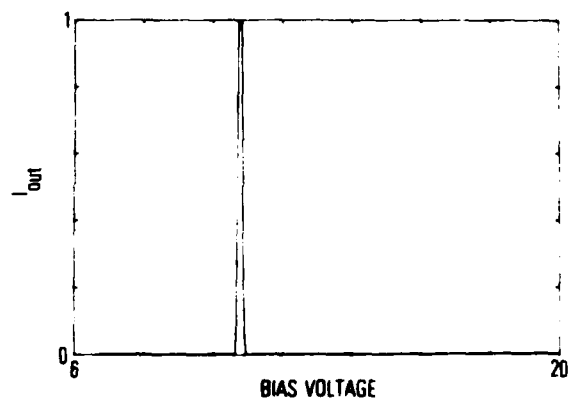
Figure 6. Contrast inverter response to intensity notch input
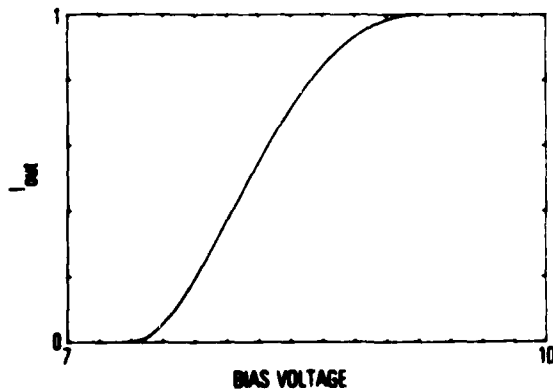
Figure 7. Temporal weighter transfer function
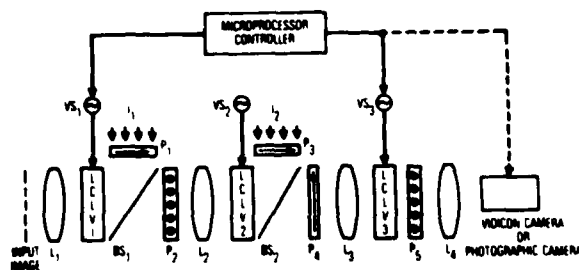
Figure 8. Experimental nonlinear image processing system
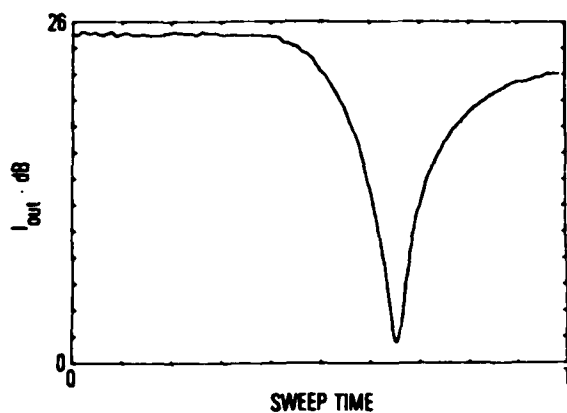
Figure 9. Experimental notch generator
response
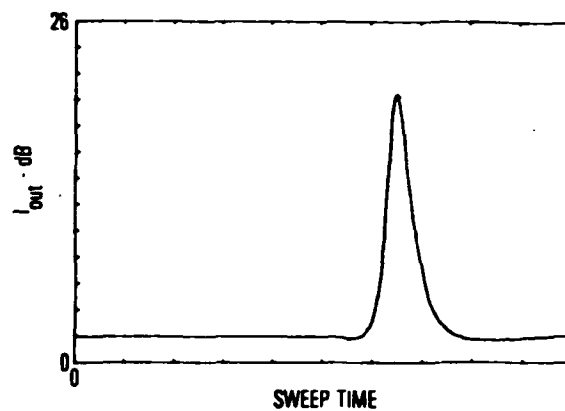
Figure 10. Experimental contrast inverter
response
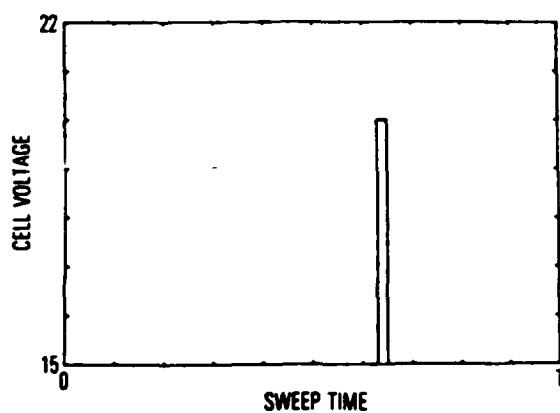
Figure 11. Temporal weighter control voltage
for level slice operation
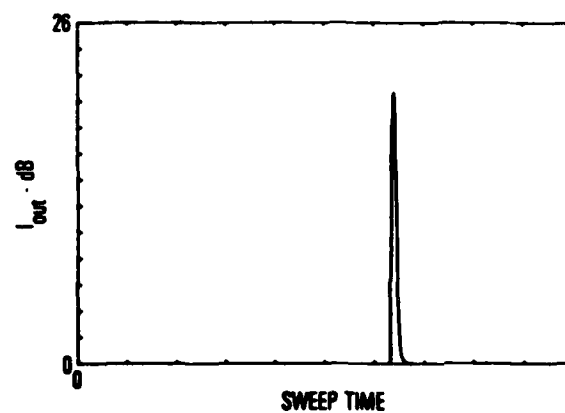
Figure 12. Preintegrated output response
for level slice operation
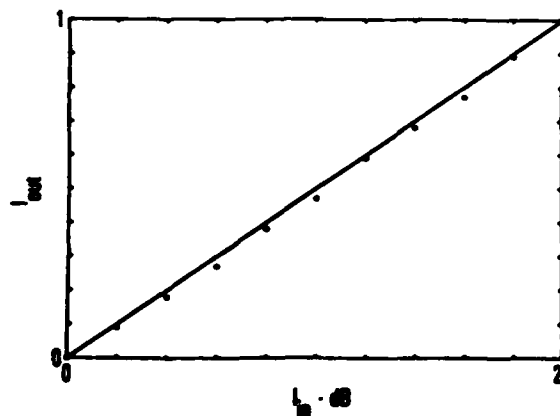
Figure 13. Logarithm operation response
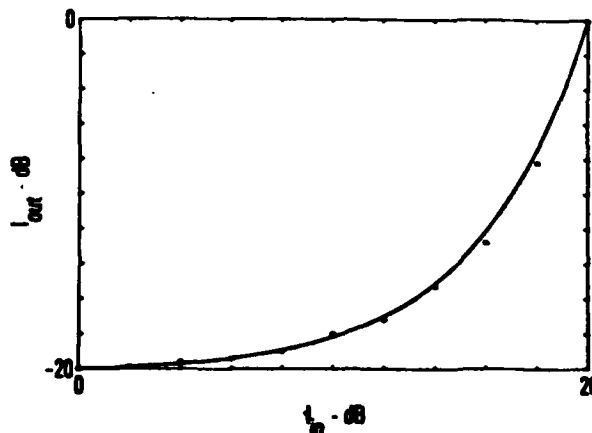
Figure 14. Exponentiation operation response
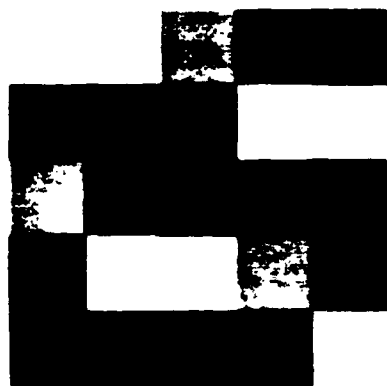
Figure 15.   Discrete intensity test image   Figure 16.   Level slice of test image
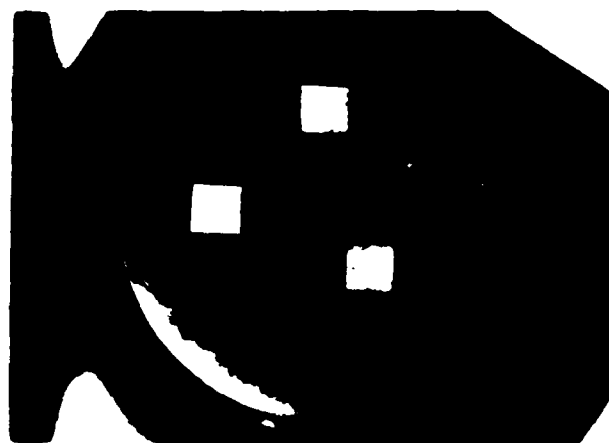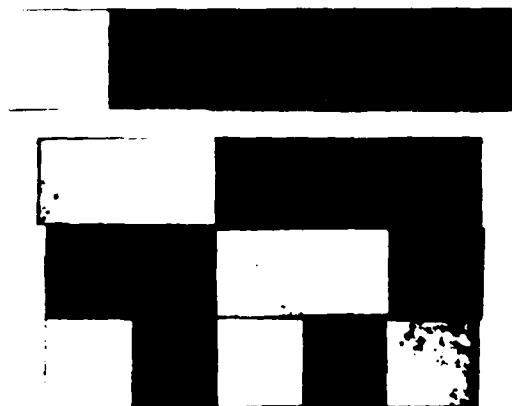
Figure 17.   A/D conversion of middle row of test image

1.6 Variable Grating Mode Liquid Crystal

Devices: Modeling

The variable grating mode (VGM) liquid crystal device [32], [37], [40], [41] has been further studied experimentally and theoretically in the last year. This work has been in conjunction with the device development work being done at HRL.

Research on variable grating mode (VGM) liquid crystal devices has produced exciting results in two principal areas: device physics and applications. This section describes a few preliminary results on device physics, and the next section describes applications for analog and digital logic processing.

In the device physics area, experiments on the intensity and polarization states of diffraction orders have been performed as a function of input polarization state. The results of these experiments can be summarized as follows (linear input polarization is assumed): the odd diffraction orders are polarized linearly parallel to the VGM domains and their strength is directly related to the parallel component of the input polarization; the even diffraction orders are linearly polarized with a 180° relative phase shift induced between the polarization components parallel and perpendicular to the VGM domains. These results were then correlated with high resolution polarizing microscope studies of an electrically activated VGM cell. The goal is to produce a model of the static or dynamic liquid

crystal director pattern within the domains, so that an accurate physical picture of the VGM effect can be obtained.

A static model of the VGM has been developed which qualitatively reproduces the observed diffraction phenomena. A computer program has been implemented to see how well predictions from the model match measured diffraction efficiencies on a quantitative basis. The model assumes that the liquid crystal director orientation rotates both in the plane of the liquid crystal device and out of the plane as one moves through one period of the grating structure. The director thus sweeps out a cone in one period of the grating. The axis of the cone coincides with the director axis when no voltage is applied. The cross section of the cone orthogonal to the axis of the cone is in general elliptical in shape.

Using the maximum value of the two rotation components of the director as parameters, the model predicted diffraction intensities for the first five orders which agreed with the measured values with less than ten percent error. In fact, the error was only slightly higher than the measurement error.

Work is in progress to refine the model and to perform additional experiments to identify additional aspects of the model which are not uniquely specified at this point.

A paper, "Variable Grating Mode Liquid Crystal Device for Optical Processing," presented at the SPIE Los Angeles Technical

Symposium in February 1980 [37] is included as a concise summary of VGM physical parameters and construction details.

Variable grating mode liquid crystal device for optical processing

B. H. Soffer, D. Boswell, A. M. Lackner

Hughes Research Laboratories, 3011 Malibu Canyon Road, Malibu, California 90265

A. R. Tanguay, Jr., T. C. Strand, A. A. Sawchuk

University of Southern California, Los Angeles, California 90007

Abstract

In the variable grating mode (VGM) operation of a liquid crystal device, a phase grating is formed whose period depends upon the voltage placed across the cell. Typical spatial frequency variation is from 100 to 600 cycles/mm. By adding a photoconductive layer to the cell, the grating period can be optically controlled. Thus each input intensity level in an optical signal will generate a local grating structure at a different spatial frequency. If the VGM device is placed in the input plane of a coherent optical processor, each point in the Fourier transform domain will correspond to a different grating frequency, and thus to a different input signal level. By varying the attenuation at each point in the Fourier plane, any desired transformation of input intensity to output intensity can be achieved. In particular, level slicing can be achieved by placing a slit in the filter plane so that only a narrow range of spatial frequencies is transmitted and thus a narrow range of input intensities is passed. Several experimental VGM real-time devices have been constructed and the results of a level slicing experiment are presented. This device has the potential to perform a wide variety of real-time, parallel, optical processes.

***

We are investigating the feasibility of using the variable grating effect for nonlinear optical data processing. Separately the possible mechanisms responsible for the VGM are being investigated. Liquid crystals exhibit domain structures; these are particularly evident when the liquid crystal is in the form of a thin film or when it is sandwiched between planar electrodes. Domain structure, which manifests itself by periodic reorientation of the optical axis of the liquid crystal, may be seen when no external electric or magnetic fields are applied or when electrohydrodynamic or magnetohydrodynamic instabilities are induced by a field. In particular, a nematic-phase liquid crystal, sandwiched between electrodes spaced 12 μm or less and with a static electric field normal to the electrodes, exhibit domains that appear as parallel structures. These domains extend along the direction of quiescent state alignment of the liquid crystal on the electrode surface, this alignment having been induced by rubbing or other appropriate methods. These domains have the unique property that they can act as phase diffraction gratings, the grating constant being a function of the applied voltage.

Cells were fabricated from plane electrodes that had been coated with ITO to provide a conductive surface. Mylar spacers were used, and cell parallelism was determined on an interferometer to be within one-half a fringe. Observations on domains were done with a polarizing microscope. A phase contrast microscope was also used, but produced no observably different results. Alignment on the surface was induced by rubbing or with an ion bombardment etch-alignment method.

VGM domains have previously been observed in planar cells.[1,2,3] We also observed these, but, contrary to the previous reports in the literature, we found the cell-spacing limit to be 12 rather than 6 μm. Also contrary to these reports, the domains for static fields always are parallel to the quiescent-state alignment on the electrode surface. For alternating fields, the domains (commonly known as Williams domains) are perpendicular to the quiescent state alignment.

For alternating fields of 10 Hz or higher, the cells always showed Williams-type domains. These domains exist in a narrow range above the threshold voltage because, as the voltage is raised, increased flow within the cell, by causing turbulence, causes scattering to occur. This, and the very small variation in the spacing of domains, limits the utility of this mode in any practical device.

For frequencies below 10 Hz, a mixed-mode behavior is observed, with VGM- and Williams-type domains appearing alternately. The cells also exhibit severe scattering during the appearance of the Williams domains, especially as the frequency is raised.

For static fields, there is a large linear variation in domain spacing as a function of voltage. For the azoxy compound Merck NV in a 6.3-μm cell, for example, the slope is ~8 lines/mm-V. For high-resistivity samples (10^{10} Ω/cm), little or no dynamic scattering occurred even for voltages as high as five times the threshold. Figure 1 shows a series of views of a VGM cell taken through a polarizing microscope. The predominant apparent effect is a decrease in the period of the phase grating as voltage increases. Some of the

SOFFER, BOSWELL, LACKNER, TANGUAY, STRAND, SAWCHUK
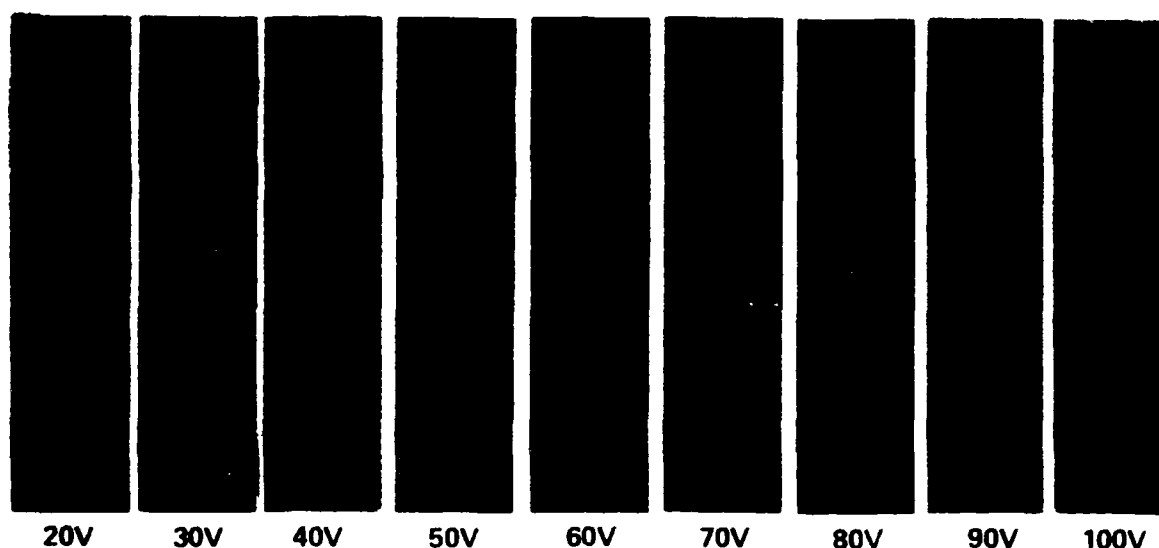
Figure 1.   VGM viewed through polarizing microscope.

typical imperfections in the VGM device can also be noted in the photographs.   There are places where two or more domains merge through arcs that, although small and not numerous, have the noticeable effect of degrading the diffraction patterns by smearing and arcing the points in Fourier space.   The remedy for this is not yet known.   Furthermore, inconsistency in the grating alignment within each picture and from picture to picture may be noted.

The diffraction patterns obtained from a typical VGM cell are shown in Figure 2.   The light beam was not well collimated in these pictures, as can be noted from the size of the zero-order spot, but the pictures serve to demonstrate the general features of the diffraction, including the development of circular arcs in the higher voltage examples.
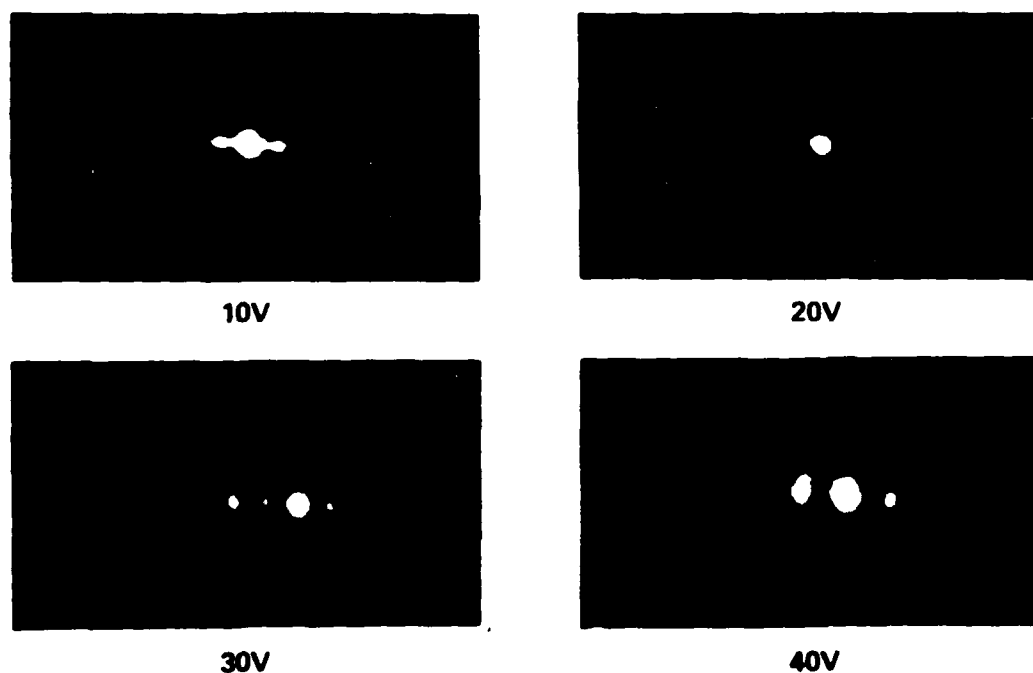
Figure 2.   Diffraction patterns of a VGM cell.

VARIABLE GRATING MODE LIQUID CRYSTAL DEVICE FOR OPTICAL PROCESSING

The diffraction efficiency of the VGM cells is >25% in 1st order. The relative strengths of the orders show that the optical phase does not vary simply sinusoidally across the grating. Interesting polarization effects are sometimes noted where all the odd orders and even orders behave differently with variation of the polarization of the light.

Preliminary work has been done on the response time. For azoxies, when switched on to a voltage above threshold, Williams-type domains appear first, accompanied by some scattering. These domains then decay into the VGM-type domains by twisting through 90° from their original direction. The process requires 3 to 4 sec. For esters, the times were as great as 15 sec. Decay time appears to vary with cell thickness.

The quality of the domains (e.g., their parallelism and the direction along which they extend) appears to depend on surface treatment. Thus, when the ITO film is coated with SiO_2 deposited at a medium angle, the domains are no longer parallel but are randomly curled in a plane parallel to the electrode surface. The grating lines in the VGM lie parallel to the liquid-crystal director. The orientation of the liquid-crystal director is enforced only by the preparation of the surfaces of the electrodes. Although rubbing has proven to be satisfactory for test cells, a much more uniform homogeneous alignment can be obtained by ion-beam etching certain types of surfaces. Figure 3 shows the best quality of domains yet obtained.

We have studied the liquid-crystal parameters relating to VGM operation to find the most suitable liquid-crystal mixture for this application. Eleven different LCs have been tested and compared so far.

The VGM effect in nematic-phase LCs of negative dielectric anisotropy has been demonstrated with azoxy mixtures, such as Merck NP V.[1,3,4] These yellow-colored eutectic mixtures from aromatic azoxy compounds absorb light in the UV and visible (below 420 nm) region of the spectrum, and they can undergo photodecomposition during long illumination. Other classes of LCs, such as phenyl benzoates, are stable to visible light with an absorption edge below 330 nm. Eutectic mixtures of these aromatic esters with varying average molecular lengths were studied for VGM under another AFOSR program (79M-0553/D7283-3).

Figure 3.   Domains in an etched cell. Magnification 100 times.

These same highly purified phenyl benzoate mixtures without dopants were tested for VGM operation and their response correlated with their average chain length, viscosity, anisotropy, index of refraction, and resistivity.

A cell was fabricated from ITO-coated, 0.5-in.-thick optical flats and a 6-µm Mylar spacer sandwiching the LC. The effect of dc voltage was observed with a polarizing microscope at 258x magnification for each LC mixture. The domain width d is inversely proportional to applied voltage according to:

$$d = o/V$$

where o is a constant that is dependent on the particular LC mixture. This relationship is best shown in Figure 4, where dc voltage versus grating period $1/d$ for each eutectic is a straight line with a slope of o^{-1}. The period of domain structure depends mainly on the sample thickness ℓ, and less on other parameters according to[5]

$$d = 0.8(\beta/\rho k_{11})^{1/4} \ell \ ,$$

where

ρ = density of LC

k_{11} = elastic constant for splay

β = viscosity coefficient.
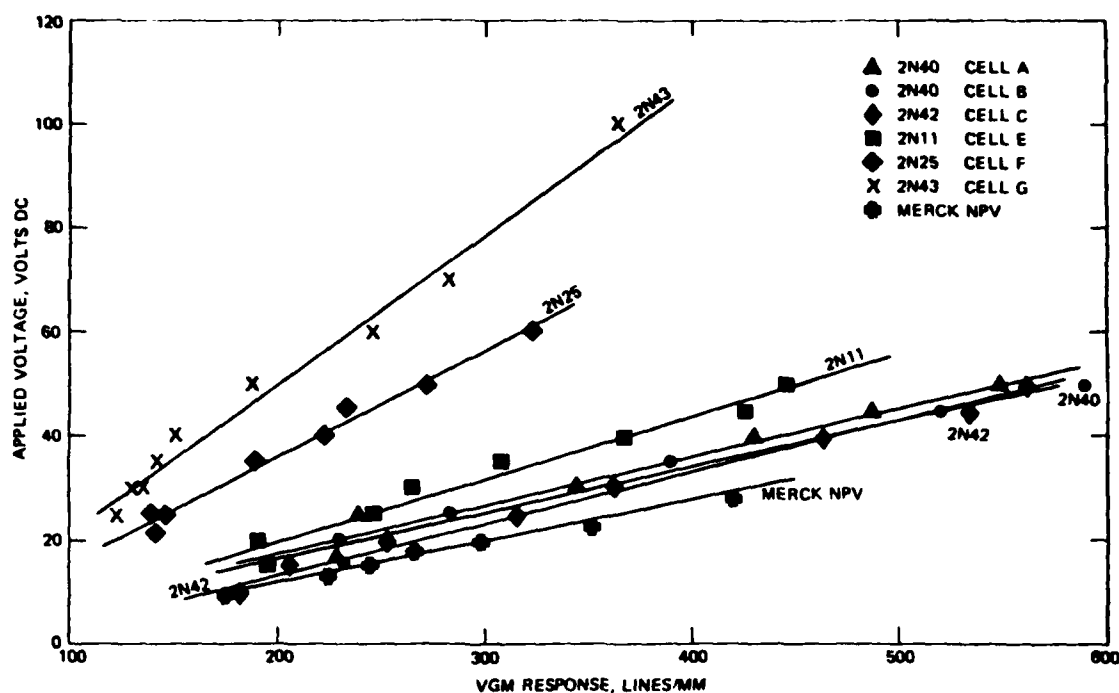
Figure 4.   VGM voltage dependence for various LCs.

Some of these parameters suggest that, for the best VGM response (i.e., maximum grating period/volt):

- Average molecular length should be minimum
- Conductivity anisotropy should be high
- Large Δn is preferred
- Range of LC resistivity 2×10^{10} to 1×10^{11} Ωcm
- Not dependent on viscosity

Research was performed on the photoconductive layer for the VGM photoactive cell.

The structure of the present photoactivated device is shown schematically in Figure 5. It includes a sputter-deposited ZnS photoconductor, and a liquid-crystal layer. These are between indium-tin oxide (ITO), transparent electrodes that have been deposited on glass substrates. A low-voltage dc drive voltage is impressed across the electrodes.

The operating principle of the device is straightforward. The thin-film structure is designed to accept most of the drive voltage when the photoconductor is not illuminated; the portion of the voltage that falls across the liquid crystal is below the activation threshold of the liquid-crystal VGM effect. When light falls on the photoconductor, the photoconductor's impedance drops, thereby switching the voltage from the photoconductor onto the liquid crystal and driving the liquid crystal into its activated state. Thus, the photoconductor acts as a light-activated voltage gate. The high lateral impedance of the thin films causes there to be very little spreading of the light or of the associated liquid-crystal electrooptic effect. As a result, the light-activation process is a high-resolution process, and the device can accept photographic-quality images.

Figure 5.   Schematic VGM cell.

VARIABLE GRATING MODE LIQUID CRYSTAL DEVICE FOR OPTICAL PROCESSING

The VGM phenomenon is a dc electrohydrodynamic instability effect occuring in high-resistivity ($\rho > 10^{10}$ Ωcm), pure liquid-crystal compositions. They re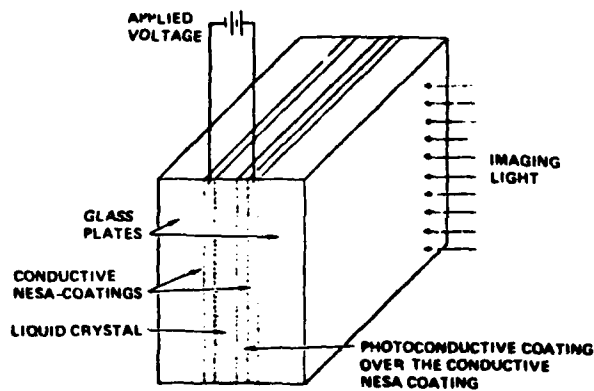quire high-impedance photoconductor layers. Zinc sulfide photoconductor has been selected for the best impedance match with the LC. Unfortunately, its photosensitivity is in the blue and uv region of the spectrum, where the LC molecules are sensitive to photodecomposition.

The ZnS layer is deposited on conductive ITO electrodes by evaporation or ion-beam-sputtering methods. With the evaporation technique, we produced photoconductors of 1.5 to 5 μm thickness, while the sputtered films were only 5,000 Å thick, highly transparent smooth surface layers. The evaporated 1.5 to 5 μm ZnS photoconductors had a hazy, rough surface appearance causing difficulties in LC alignment parallel to the electrodes. It has been reported that vaporized ZnS causes homeotropic or tilted homeotropic orientation of the LC material.[6] Mechanical polishing of the evaporated photoconductors increased their transparency and surface uniformity, while polymer (PVA) coating the top of these ZnS layers, supplemented by additional surface treatment, resulted in good parallel alignment. Photo-sensitive devices were fabricated from the vapor-deposited and sputtered ZnS using ITO counter electrodes and 6-μm spacers. The photoconductors were evaluated and compared by measuring the dark current and switching ratios of the VGM devices. The photojunctions sometimes observed can help to increase the effective switching ratio of current with and without illumination. In Figure 6, the behavior of one such junction is plotted. It resembles the behavior of two photojunctions back to back. At a certain bias, this cell crossed over through zero switching ratio (for the illuminations shown) and reversed to a negative ratio! A layer-by-layer study of the elements of the cells is being done to determine the nature of these junctions. From the results, for devices with switching ratios above 6, the dark current has to be less than 6×10^{-9} A-in.$^{-2}$, and this low dark current is obtained with sputtered as well as evaporated ZnS.
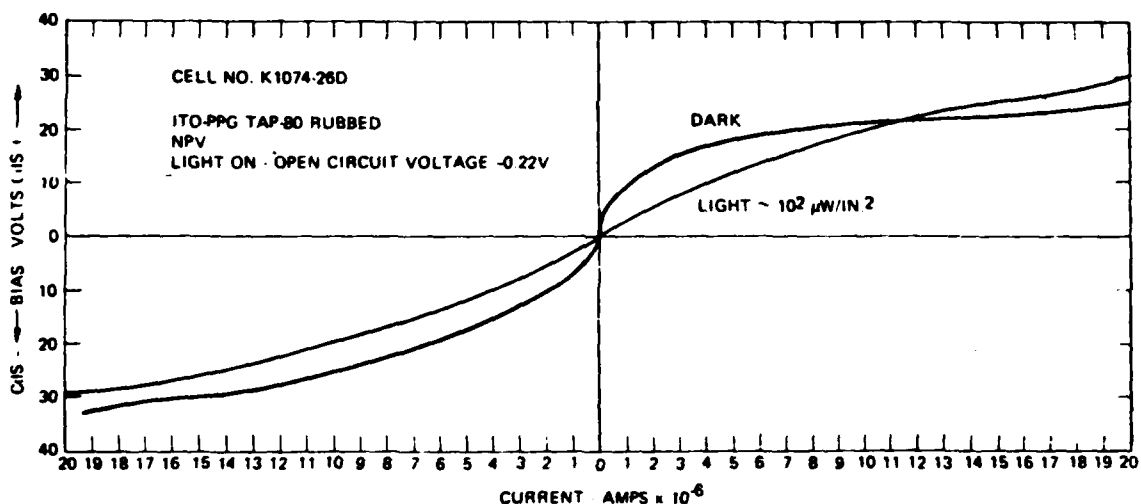
Figure 6. Junction effect in VGM cell.

VGM cells were studied with respect to edge effects on resolution and possible "spillover" of domains into adjacent unactivated areas. Electrodes were specially prepared by removing sections of the conductive coating by etching. A parallel plate cell was constructed such that there were conductive areas facing each other, either with conductive edges aligned or with a maximum overlap of 150 μm of a conductive electrode over the nonconducting area. Cell spacing was 6.3 μm, and the material was Merck NV. For alignment parallel to the edge when operating close to the threshold voltage, domains were parallel to the edge and within the active area. For higher voltages, there was fringe spillover by not more than one fringe spacing. For alignment perpendicular to the edge, domains appear to either terminate at the edge or to join with an adjacent domain. The quality of the edge behavior is shown in Figure 7.

The results indicate that a VGM light valve is a viable device requiring dc operation. Studies of the edge effects indicate that implementation of the VGM in an image-processing device should ultimately produce excellent resolution.

From the preliminary photosensitive devices
fabricated using a ZnS photoconductor layer to
achieve the high impedance needed, one cell
was selected that aligned well and did not
suffer the usual rapid deterioration seen in
dc operation. This deterioration supposedly
results from poisoning the LC by the diffusion
of ions from the photoconductor. The cell was
biased negatively on the photoconductor. This
cell was protected as much as possible from
short wavelength illumination although this
was not entirely possible since ZnS requires
blue to long UV for photoexcitation. This
particular cell was constructed of a 5-μm-
thick evaporated ZnS layer that had been
polished and then rubbed with surfactant poly-
vinyl alcohol. The 6-μm-thick LC layer was
made of Hughes 2N40 ester. The counter elec-
trode was an ITO transparent layer treated with
the same surfactant. The series impedance was

Figure 7. Behavior of domains near
an edge. Magnification 100 times.

measured to be ~3 x 10^8 Ω. With 160 V applied and with the maximum available illumination
at 7.3 mW/cm^2 in the passband 410 to 550 nm, the periodicity of the VGM was calculated from
the diffraction to be 588 lines/mm. The device threshold at this illumination was 21 V,
corresponding to a grating periodicity of 103 lines/mm. The optical threshold at 160 V is
~50 μW/cm^2, and the device appears saturated at 7.5 mW/cm^2. Saturation behavior remains to
be studied. With an image on the photoconductor surface of the device, a mapping into local
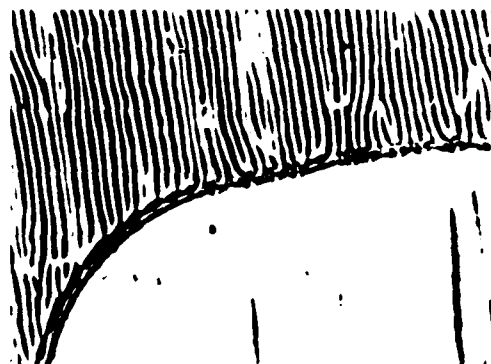intensity dependent periodicities is produced in the LC layer.

Intensities can be mapped, within the dynamic range of the device, monotonically into
positions along a line in Fourier space by an optical transform. Departures from the line
may be caused by imperfections in the alignment of the induced grating direction. The
spatial positional information is coded into phase and sidebands in two dimensional Fourier
space. A new parameter, the intensity, has thus been coded into Fourier space. Since the
periods of the VGM are much finer than the periods encountered in the images to be processed,
we are in a tractable situation, familiar in communications, where the carrier frequency is
higher than the modulation frequencies. Optical filtering should produce a variety of linear
and nonlinear image transformations. One such transform, isophote contouring (or level slic-
ing) is described below.

For a first example of the use of the VGM device, we have successfully demonstrated level
slicing of a continuous-tone image using simple Fourier filtering. Small circular annuli
of varying radii were used to select particular intensities or level slices. Figure 8 shows
a series of such slices. Figure 8(a) shows a positive print of the original image as photo-
graphed on the imaging screen. The negative was used in the experiments. Figure 8(b) shows
a low-intensity level slice corresponding to a VGM periodicity of 120 lines/mm with ~3% band-
width. In Figure 8(c), another level, corresponding to 153 lines/mm, is shown. Figure 8(d),
at 236 lines/mm illustrates an ambiguity not mentioned before. Weak second harmonics of the
low-intensity image slice corresponding to 118 lines/mm can appear in the 236-lines/mm level
slice. It should be possible to resolve this ambiguity by subtraction or by other schemes.
In Figure 8(e), a broader slice of 11% bandwidth was taken centered about the level corre-
sponding to 140 lines/mm. This picture may be compared with the previous slices and parti-
cularly with the slice shown in Figure 8(c). Finally, Figure 8(f) shows a very high inten-
sity slice at 440 lines/mm of 10% bandwidth. Three gray levels may be seen simultaneously;
these correspond to the superposition of three wide-intensity slices.

Acknowledgments

References

1. J.D. Margerum et al., Phys. Lett. 19, 216-218, October 1971.
2. W. Grenbel and V. Wolf, Appl. Phys. Lett. 19, 213-215, October 1971.
3. J.M. Pollack and J.B. Flannery, SID 76 Digest, pp. 143-145. University of Southern
California Image Processing Institute Report 720, 30 September 1976.
4. P.K. Watson, J.M. Pollack and J.B. Flannery, "Liquid Crystals and Ordered Fluids,
Vol. 3, p. 421, (1977).
5. I.G. Chistyakov and L.K. Vistin, Sov. Phys. Crystallogr. Vol. 19, No. 1, July-Aug
(1974).
6. H. Kruger, H.F. Mahlim, and W. Raushcer, U.S. Pat. 4,112,157,05 Sept. 1978.

VARIABLE GRATING MODE LIQUID CRYSTAL DEVICE FOR OPTICAL PROCESSING
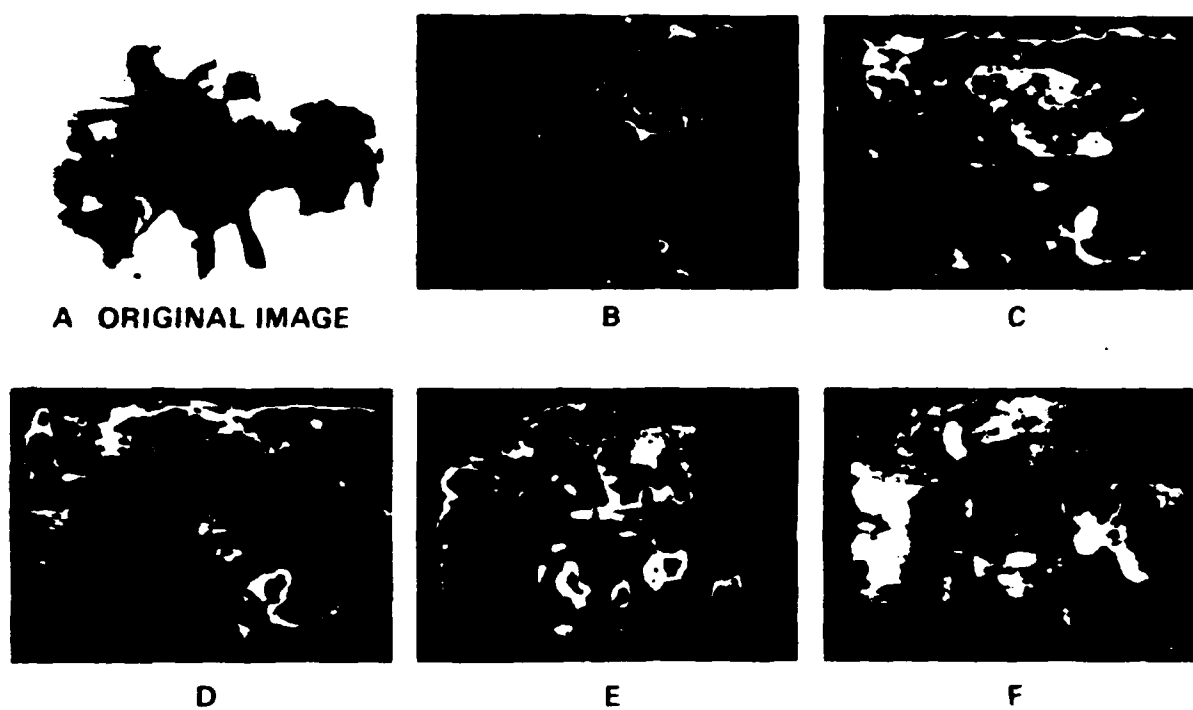
Figure 8.   Level slicing with the VGM LCLV.

1.7 Variable Grating Mode Liquid Crystal

Devices: Applications

Several new areas of applications for VGM devices have been recently investigated, including optical digital logic functions, full adder, and matrix operations. The new discovery here consists in realizing that any intensity-to-spatial frequency conversion scheme such as the VGM device can be readily utilized for numerous other optical processing technologies in addition to direct nonlinear function implementation. In the optical digital logic application, a VGM cell was shown to be capable of producing any positive or negative digital logic operation (AND, OR, NOR, NOT, NAND, XOR, NXOR, etc.) merely by changing a Fourier plane filter. This approach satisfies the long-sought optical computer requirements of programmable flexibility and level restoration. In addition, for three superimposed input binary bit planes (two input planes and a carry bit plane), the VGM device allows a full adder (sum bit and carry bit) to be implemented in a single pass through a single device.

A major aspect of the work with optical logic which has not been reported in the literature is an attempt to fabricate a complete optical circuit using a liquid crystal device.

Given that any resolution element on a liquid crystal device can act as a logic gate, in order to build a circuit, one need only to have a means of interconnecting the gates. This is done

using a single device in a feedback loop. The feedback loop contains a computer generated hologram which takes the light from each gate (from the read side of the device) and redirects it to one or more different gates on the write side of the liquid crystal device. Thus, many elements can be easily interconnected and the entire logic array can be programmed by changing the computer generated hologram in the feedback loop. Initial experiments are under way to implement a ring oscillator and a master-slave flip-flop. This work is continuing and will be reported on in the near future.

Details of the most recent work are contained in two papers, "Optical Computing with Variable Grating Mode Liquid Crystal Devices," presented at the SPIE Technical Symposium East/1980 Optical Computing Conference, in April 1980 [40], and "Optical Logic with Variable-Grating-Mode Liquid-Crystal Devices," published in September 1980 Optics Letters [41]. These papers are included here.

OPTICAL COMPUTING WITH VARIABLE GRATING MODE LIQUID CRYSTAL DEVICES

B.H. Soffer, D. Boswell, A.M. Lackner
Hughes Research Laboratories
3011 Malibu Canyon Road
Malibu, California 90265

P. Chavel, A.A. Sawchuk, T.C. Strand, and A.R. Tanguay, Jr.
Image Processing Institute
University of Southern California
Los Angeles, California 90007

Abstract

A liquid crystal device that performs a two-dimensional intensity-to-spatial frequency conversion has been developed for use as an optical transducer. When such a device is used as the input transducer in an optical filtering arrangement, image intensity levels can be easily manipulated via Fourier plane filters. This variable input intensity-output intensity transfer function has numerous potential applications in image processing. Implementation of a variable level slice operation is discussed and experimental results presented. The VGM LCLV device is also particularly well adapted to performing binary logic operations on 2-D images. This application is discussed, and results demonstrating the implementation of common logic operations are presented.

Introduction

One of the primary concerns in the fields of optical image processing and optical computing is the desire for a wider range of real-time input transducers to meet the special requirements of various processing schemes. Variable-grating-mode (VGM) liquid crystal devices offer a radically new approach to the problem of optical transducers[1]. The basic function of the VGM device is to perform an *intensity to spatial frequency* conversion. This is done simultaneously over a two-dimensional image field so that the intensity variations of an image are converted to local spatial frequency variations in a phase grating structure within the liquid crystal layer. Due to the intensity-to-spatial frequency conversion thus performed, a standard spatial filtering system can be used to manipulate the VGM spatial frequencies and thus the input intensities. In this paper we describe two basic applications of the VGM device: nonlinear processing of continuous tone images and optical logic operations on binary images. The VGM liquid crystal light valve has many advantages for both of these processes.

The ability to perform arbitrary point nonlinearities over two-dimensional images greatly increases the flexibility of optical processing systems[2]. In the past few years several different approaches to the problem of implementing generalized nonlinearities have been investigated[3]. These have included halftone screen techniques[3,4,5,6] nonlinear devices[7,8], feed back methods[9], and a variable level slice[10] among others. The main advantage of the VGM approach over previous methods is the ease of programming the functional nonlinearity desired for a given image transformation. This is done simply by changing the transmittance distribution of the spatial filter in the optical processing system. The spatial filter is relatively low resolution and need only have a space-bandwidth product equal to the number of gray levels to be processed independent of the space-bandwidth product of the input image.

The same programmability advantage applies to the implementation of binary logic operations. One device can be used to implement any of the common logic operations (AND, OR, XOR, and their complements) by simply changing a Fourier plane filter. Previously described optical logic systems were "hardwired" to perform specific operations[11,12,13], and in most cases one or more logic functions proved difficult or cumbersome to implement.

A second major advantage of the VGM system is the possibility for level restoration at each stage in order to provide required noise immunity. This capability has been lacking in other numerical processing systems where noise accumulates in cascaded stages.

It should perhaps be pointed out that considerable effort has been directed toward using integrated optics for logic elements[14,15,16]. This approach is inherently one-dimensional and does not fully exploit the advantages available to fully parallel two-dimensional optical processing algorithms.

In the following we first describe the basic principles of operation of the VGM device. Then we discuss in more detail how it can be used for nonlinear processing of images and some of the limitations of device performance. A variable level slice experiment is discussed as an example of nonlinear processing. Next, the application of the VGM device to logic operations is introduced and some preliminary experimental results are presented.

VGM device description

The primary active element of the variable grating mode liquid crystal device is a thin layer of liquid crystal that is observed to form periodic stripe domains in the presence of an applied voltage [1] as shown in Fig. 1a. The formation of the domains results in a phase grating characterized by a spatial frequency that depends on the magnitude of the voltage across the liquid crystal layer. The grating period can be optically controlled by placing a two-dimensional photoconductive layer in series with the layer of liquid crystal.

The structure of the present photoactivated device is shown schematically in Fig. 1b. It includes a sputter-deposited ZnS photoconductor, and a liquid-crystal layer. These are sandwiched between indium-tin oxide (ITO) transparent electrodes that have been deposited on glass substrates. A low-voltage dc drive voltage is impressed across the electrodes.

The operating principle of the device is straightforward. The thin-film structure is designed to accept most of the drive voltage when the photoconductor is not illuminated; the portion of the voltage that falls across the liquid crystal is below the activation threshold of the liquid-crystal VGM effect. When light falls on the photoconductor, the photoconductor's impedance drops, thereby switching the voltage from the photoconductor onto the liquid crystal and driving the liquid crystal into its activated state. Thus, the photoconductor acts as a light-activated voltage gate. The high lateral impedance of the thin film causes there to be very little spreading of the photoconductivity or of the associated liquid-crystal electrooptic effect. As a result, the light-activation process is a high-resolution process, and the device can accept photographic-quality images.

Nonlinear processing of continuous valued signals with the variable grating mode liquid crystal device

The VGM liquid crystal device can be considered to be an intensity-to-spatial frequency converter capable of operating on two-dimensional images. The intensity-to-spatial frequency conversion allows the implementation of arbitrary point nonlinearities with simple Fourier plane filters. As discussed above, when an input image illuminates the photoconductor surface of this device the intensity variations of the input image change the local grating frequency. If coherent light is utilized to Fourier transform the processed image, different spatial frequency components (corresponding to different input intensities) of the encoded image appear at different locations in the Fourier plane as shown in Fig. 2a. Thus, by placing appropriate spatial filters in this plane it is possible to obtain different transformations of the input intensity in the output plane as depicted in Fig. 2b. This figure describes the variable grating mode nonlinear processing graphically. The input intensity variation is converted to a spatial frequency variation by the characteristic function of the VGM device (upper right-hand quadrant). These variations are Fourier transformed by the optical system and the spectrum is modified by a filter in the Fourier plane (upper left-hand quadrant). Finally, a square-law detection produces the intensity observed in the output plane (lower left-hand quadrant). Considered together, these transformations yield the overall nonlinearity (lower right-hand quadrant). Design of a proper spatial filter for a desired transformation is a relatively easy task. For example, a level slice transformation requires only a simple slit that passes a certain frequency band or bands. A mathematical formulation of nonlinear processing utilizing the VGM device is presented in the next section.

Variable phase grating analysis

Consider a phase grating (periodic array of phase shifting elements) extending to infinity in both the x and y directions. Let $g(x,y)$ be the complex amplitude transmittance of the phase grating. Since the grating extends to infinity we can assume that $g(x,y)$ is a periodic function of x and write it as a Fourier series expansion

$$g(x,y) = \sum_{n=-\infty}^{\infty} c_n \exp(j2\pi nx/L) \tag{1}$$

where

$$c_n = \frac{1}{L} \int_0^L g(x,y) \exp(-j2\pi nx/L) dx \tag{2}$$

and L is the period of the grating. Because we assume that the grating extends to infinity in the y-direction, $g(x,y)$ is not an explicit function of y.

For the case of a uniform input intensity distribution and a Fourier plane filter $\underline{H}(fx,fy)$ which transmits only the first diffraction order, it can be easily shown that the output intensity, I_0, resulting from the inverse Fourier transform is

$$I_0(x,y) = |\underline{c}_1 \underline{H}(\frac{1}{L},0)|^2 \tag{3}$$

where $\underline{H}(\frac{1}{L},0)$ is the filter amplitude transmittance at the first diffraction order of the VGM grating with period L and $\underline{c}$ is a constant. Thus the output intensity is directly related to the variation in the filter transmittance as a function of spatial frequency.

Using the above analysis, the processing limitations of the VGM device can be estimated. The fundamental question to be answered is how large the smallest picture element, or pixel, must be with respect to the VGM grating frequency.

Suppose that the usable spatial frequency range over which the VGM device can operate is $\delta\nu_o$. To avoid crosstalk from higher diffracted orders the VGM device can only be operated between the first diffraction order and the next non-zero harmonic of the lowest fundamental frequency. Experiments indicate that the second harmonic can be eliminated by a polarizing filter so that the third harmonic is the next non-zero component. However, in the subsequent derivation if it is assumed that the second order sets the limiting frequency for a "worst case" calculation. If the lowest frequency used is denoted by ν_o then the usable frequency range is

$$\delta\nu_o = 2\nu_o - \nu_o = \nu_o \tag{4}$$

as shown in Fig. 3. If the number of intensity levels that must be distinguished is N, then the Fourier transform of any one aperture represented by $2\Delta\nu$ in Fig. 3 must be contained within a region of width ν_o/N in the Fourier plane. So we must have

$$2\Delta\nu \leqslant \nu_o/N. \tag{5}$$

If the pixel width is b, then the width of its Fourier transform is 2/b, which implies that

$$2\Delta\nu = \frac{2}{b} \tag{6}$$

Combining Eg. (5) and (6) we have

$$\frac{2}{b} \leqslant \nu_o/N \tag{7}$$

or

$$b\nu_o \geq 2N. \tag{8}$$

This relation thus requires that the pixel size contains 2N periods of the lowest grating frequency if N grey levels are to be processed. For example, if $\nu_o = 200$ cycles/mm and $N = 50$, then each pixel must have a size $b = 0.5$ mm. Thus if the device has a 50 mm square area a 100 x 100 pixel image could be processed with 50 defined grey levels.

Demonstration of a level slice function with the VGM device

In this experiment the ability of the VGM device to generate a level-slice nonlinearity is demonstrated. The experimental setup is shown in Fig. 4. The input picture is illuminated by an arc lamp source and imaged onto the photoconductor surface of a VGM device which initially has a uniform phase grating structure due to a dc bias voltage. The grating period is locally modulated by the input picture intensity, and this modulation is mapped into a position along a line in the spatial filter plane. A red filter ensures that only the readout laser beam enters the coherent optical processor. Small circular annuli of varying radii are used to pass certain spatial frequency bands. This in effect allows only prescribed input intensity ranges to appear in the output. Figure 5 shows both the input and level sliced output pictures. Figure 5a shows a positive print of the original image as photographed on the imaging screen. A negative of the original was used in the experiments. Figure 5b shows a low intensity level slice corresponding to a VGM periodicity of 120 lines/mm with approximately 3% bandwidth. In Fig. 5c another level, corresponding to 153 lines mm, is shown. Figure 5d of the

lines/mm, illustrates the interference from second harmonics. Weak second harmonics of the low-intensity image slice corresponding to 118 lines/mm can appear in the 236 lines/mm level slice. In Fig. 5e, a broader slice of approximately 11% bandwidth was taken centered about the level corresponding to 140 lines/mm. This picture may be compared with the previous slices and particularly with the slice shown in Fig. 5c. Finally, Fig. 5f shows a very high input intensity slice at 440 lines/mm of 10% bandwidth. Three grey levels may be seen simultaneously; these correspond to the superposition of three broad intensity slices.

VGM implementation of logic functions

To see how the VGM device can be used to implement logic operations, one need only realize that the function of a logic circuit can be represented as a simple binary nonlinearity. The input-output characteristics of the common logic functions are shown in Fig. 6. The input in these figures is assumed to be the simple arithmetic sum of the two input logic levels. Thus NOT is simply a hard-clipping inverter, AND and OR are hardclippers with different thresholds and XOR is a level slice function. Any spatial light modulator or optical processing system which can produce these nonlinearities can be used for implementing combinatorial logic. Furthermore, if the system allows feedback to be readily introduced, sequential or latching logic can also be implemented.

The VGM device is well suited to implementing these nonlinearities. With the VGM approach, nonlinearities are obtained using a Fourier plane filter whose transmittance variation in one-dimension is essentially a plot of the desired nonlinearity. Thus arbitrary nonlinearities are easily produced and changed. For logic operations the situation is quite straightforward. Since the nonlinearities associated with logic operations are binary functions, they can be implemented with simple slit apertures, i.e., 0 or 1 transmittance values. Such binary filters are the simplest filters to implement. A second feature of the VGM technique that is especially suitable for logic processing is that the input and output are physically separate beams. The input beam modulates a photoconductor; concurrently the image is red out with a second beam. This separation of input and output provides for the possibility of restoring the output levels to the 0 and 1 values even if the input levels are not exactly correct. This feature is essential to the production of a reliable logic system that is immune to noise and systematic errors in the levels. Electronic logic elements possess such level restoring capability, but currently proposed optical logic schemes lack this essential characteristic.

Two further aspects of logic operations which are advantageous for optical implementation purposes are the facts that logic operation input levels are discrete, and that only a small number (2-4) of distinguishable levels are required. The existence of discrete input levels implies that the nonlinearities need not have the exact forms shown in Fig. 6. In particular the transition regions need not be perfectly sharp thresholds since the input values are presumed not to occur within the transition regions in any event. The fact that only a few levels need be distinguished implies that the grey-level resolution requirements for the system are minimal.

The operations discussed above are the basic combinatorial logic functions. However, sequential logic may also be implemented with appropriate feedback, i.e., imaging the output plane onto the input plane (which can be accomplished with incoherent illumination). However, with the present VGM transmission devices there is a problem of separating the read and write functions in a feedback system since their wavelengths must be identical.

Experimental results of logic implementation

A series of experiments were conducted to demonstrate the fundamental logic functions. The experimental setup of Fig. 7 was used. Two input fields were superimposed at the VGM plane along with a bias illumination. The total illumination intensity on the photoconductor of the VGM device was thus the sum of the two input intensities and the bias intensity. The input illumination was a filtered high-pressure mercury arc lamp. The bias illumination was provided by a collimated tungsten bulb source. The VGM device was read out in transmission using a HeNe laser. A filter was placed in the Fourier plane to select the desired diffraction orders for each logic function.

For these experiments, the inputs consisted of one vertical rectangular aperture and one horizontal aperture. When these were superimposed along with the bias, a square image was formed with the four quadrants having the intensity levels shown in Fig. 8. This image corresponds to the four logic truth table shown. Thus the output images have intensity levels determined by the truth table associated with the desired logic function. The logic functions AND, OR, XOR and their complements were implemented sequentially as shown in Fig. 9 by altering only the Fourier plane filter. Imperfections visible in the output arise from defects in the cell structure of the VGM device employed in these

experiments. Investigations on VGM device improvements, limitations, processing speed and pixel uniformity are in progress.

Conclusion

We have described a new type of optical transducer, the variable-grating-mode (VGM) liquid crystal device which operates by providing an intensity-to-spatial frequency conversion. It has been demonstrated theoretically and experimentally that this device can be used for implementing arbitrary nonlinearities on continuous tone images, and can be employed to perform combinatorial logic operations on binary images. The VGM approach has several advantages over other techniques. Principal among these advantages is the flexibility of the device inherent in its functional programmability, which may be exercised at will merely by changing a low-resolution spatial filter.

Acknowledgements

References

1. B.H. Soffer et al., "Variable Grating Mode Liquid Crystal Device for Optical Processing," Proceedings SPIE 1980 Los Angeles Technical Symposium, Vol. 218, Los Angeles, February 1980 (to be published).
2. J.W. Goodman, "Operations Achievable with Coherent Optical Information Processing Systems," Proc. IEEE, Vol. 65, pp. 29-38 (1977).
3. A. Armand, "Real-time Nonlinear Optical Information Processing," (Ph.D. Thesis) USCIPI Report 880, Image Processing Institute, University of Southern California, Los Angeles, California 90007 (1979).
4. H. Kato and J.W. Goodman, "Nonlinear Filtering in Coherent Optical Systems Through Halftone Screen Processes," Appl. Opt. Vol. 4, pp. 1813-1824 (1975).
5. H.-K. Liu, J.W. Goodman and J. Chan, "Equidensitometry by Coherent Optical Filtering," Appl. Optics., Vol. 15, pp. 2394-2399 (1976).
6. A. Armand, A.A. Sawchuk, and T.C. Strand, "Nonlinear Optical Processing with Halftones: Accurate Predictions for Degradation and Compensation," submitted to Appl. Opt.
7. A. Armand, et al., "Real-time Optical Analog-to-Digital Conversion," Optics Letters, Vol. 5, p. 129 (1980).
8. A. Tai, T. Cheng, F.T.S. Yu, "Optical Logarithmic Filtering Using Inherent Film Nonlinearity," Appl. Opt., Vol. 16, pp. 2559-2564 (1977).
9. B.J. Bartholomew and S.H. Lee, "Nonlinear Optical Processing with Fabry-Perot Interferometers Containing Phase Recording Media," Appl. Opt., Vol. 19, p. 201 (1980).
10. J.D. Michaelson, and A.A. Sawchuk, "Nonlinear Optical Processing Using Liquid Crystal Light Valves," Proc. SPIE 1980 Los Angeles Technical Symposium, Vol. 218, Los Angeles, February 1980 (to be published).
11. R.A. Athale and S.H. Lee, "Development of an Optical Parallel Logic Device and Half-adder Circuit for Digital Optical Processing," Opt. Eng, Vol. 18, pp. 513-517 (1979).
12. S.A. Collins, Jr., U.H. Gerlach and Z.M. Zakman, "Optical Feedback for Generating Arrays of Bistable Elements," Proc. SPIE on Optical Processing Systems, Vol. 185, pp. 36-41 (1979).
13. D.H. Schaefer and J.P. Strong, III, "Tse Computers," Proc. IEEE, Vol. 65, pp. 129-138 (1977).
14. L. Goldberg and S.H. Lee, "Integrated Optical Half-adder Circuit," Appl. Opt., Vol. 18 pp. 2045-2051 (1979).
15. S.M. Jensen, "High-Speed Optical Logic Devices," Proc. SPIE 1980 Los Angeles Technical Symposium, Vol. 218, Los Angeles, February 1980 (to be published).
16. E. Garmire, "Review of Integrated Optical Bistable Devices," Proc. SPIE 1980 Los Angeles Technical Symposium, Vol. 218, Los Angeles, February 1980 (to be published).

(a)   (b)
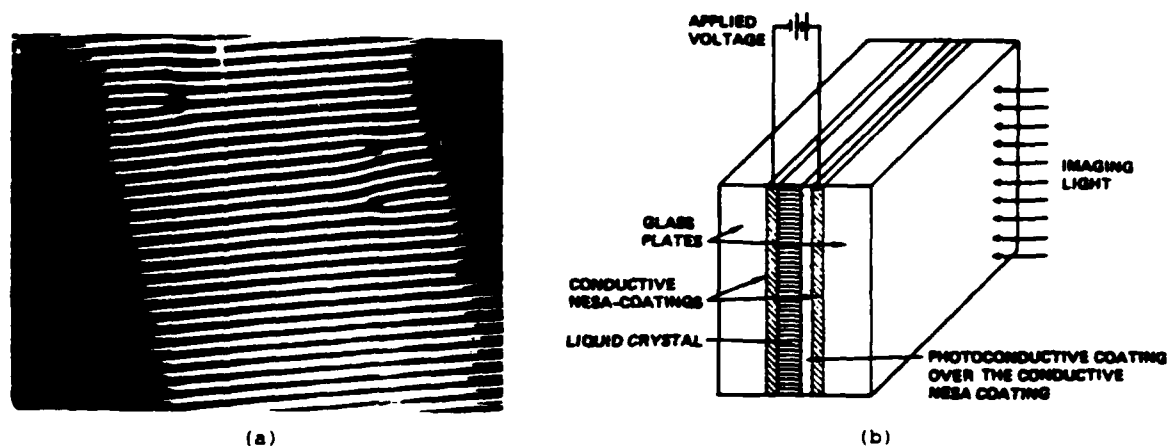
Figure 1. VGM cell. (a) The phase grating structure of the VGM device at a fixed voltage
           viewed through a phase contrast microscope. (b) Schematic diagram of the VGM
           device construction. Current devices are read out in transmission at a wave-
           length at which the photoconductor is insensitive.

Input   VGM   Filter   Output
           LCLV   Plane

(a)

(b)

Figure 2. VGM nonlinear processing. (a) Experimental setup indicating the mapping of
           intensity to spatial frequency. (b) The overall input-output characteristic
           can be found by stepping through the successive nonlinear transformations
           including (1) the intensity to spatial frequency conversion, (2) spatial
           filtering, and (3) intensity detection.

OPTICAL
FOURIER
TRANSFORM

$2\Delta\nu$

ν_0

$2\nu_0$

VGM
IMAGE

LOWEST
VGM
FREQUENCY
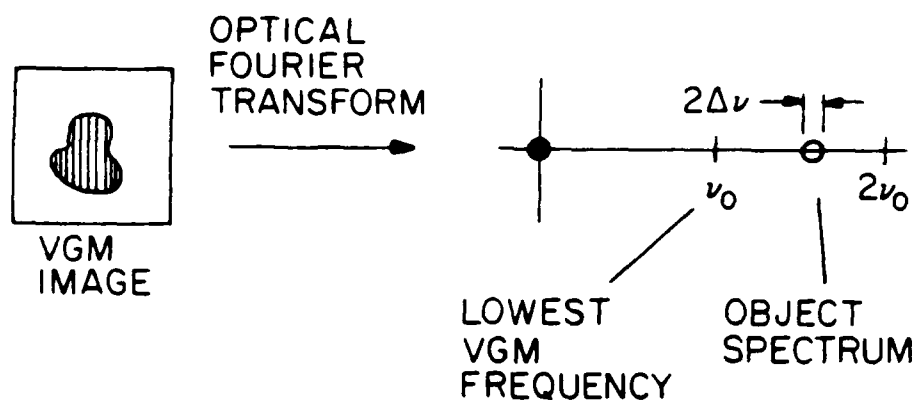
OBJECT
SPECTRUM

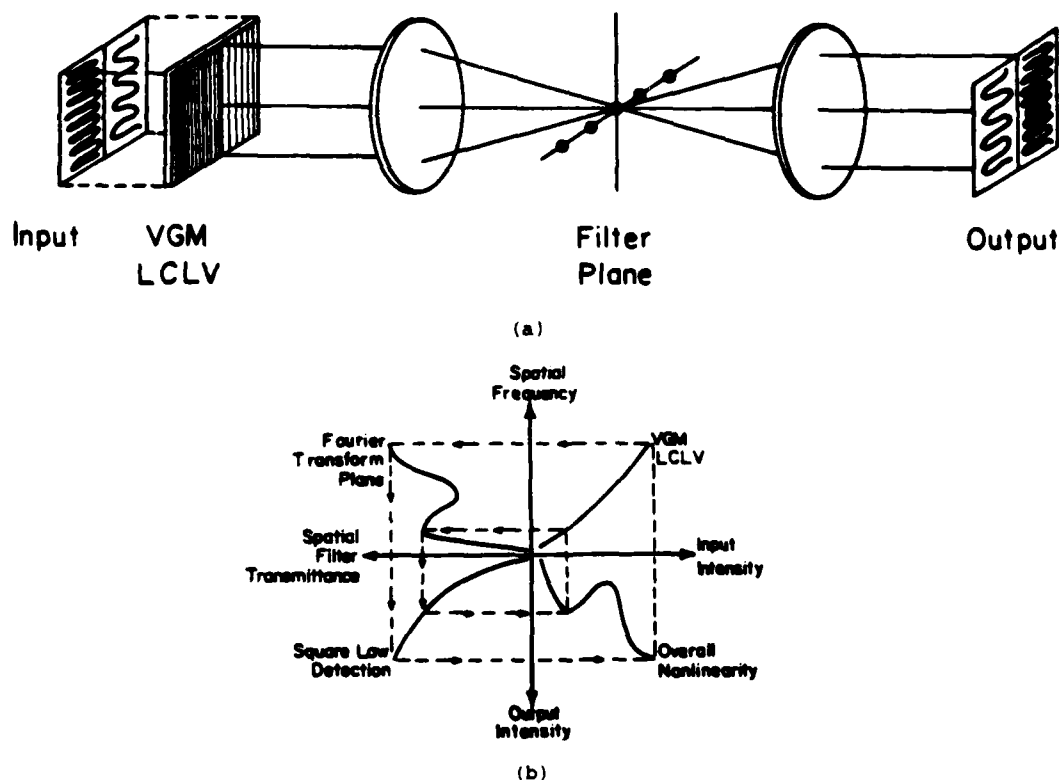Figure 3. The gray level resolution is limited by the ratio of the distance
between VGM harmonics to the object spectrum bandwidth.

INCOHERENT
LIGHT
SOURCE

DC VOLTAGE
SOURCE

OUTPUT
PLANE

INPUT
PLANE

BEAM
SPLITTER

RED
FILTER

SPATIAL
FILTER PLANE

PROJECTION LENS

VGM
DEVICE

COHERENT OPTICAL
PROCESSOR

SPATIAL FILTER

COLLIMATING LENS

50 mw
HeNe
LASER
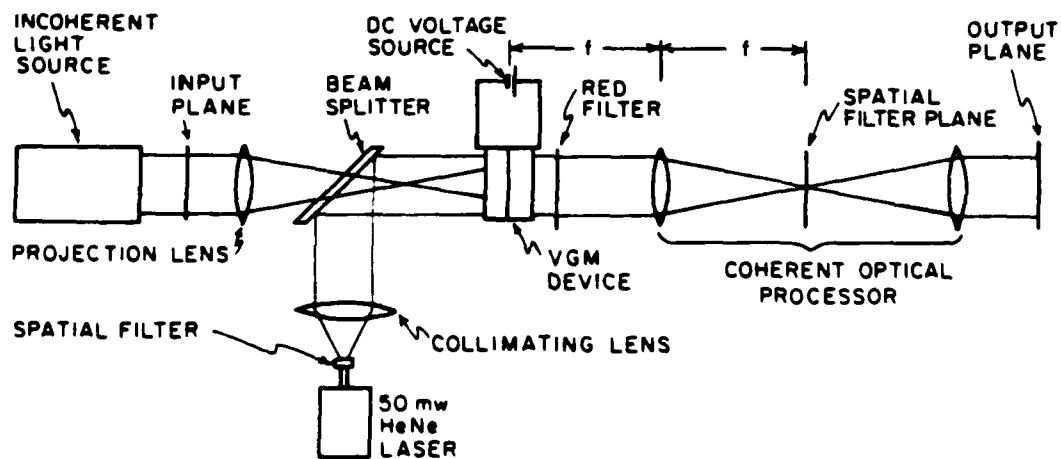
Figure 4. Experimental setup used to perform the level slice experiments.
The spatial filter was a variable annular aperture.

A ORIGINAL IMAGE

B

C

D

E

F
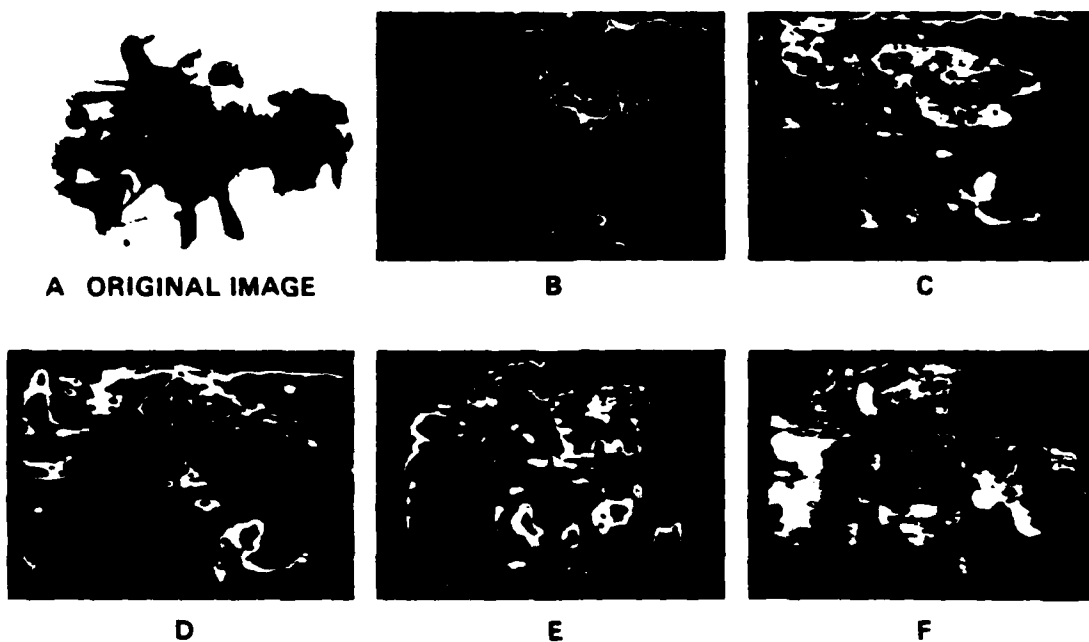
Figure 5. Level slice results. (A) Original image.
(B-F) Represent level slice results for
various apertures as discussed in the text.
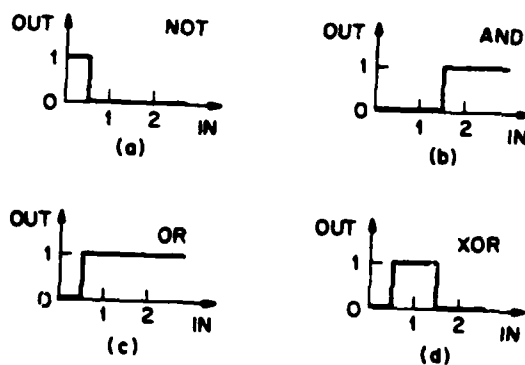
Figure 6. Logic functions as simple nonlinearities.
Given an input consisting of the sum of two
binary inputs, different logical operations
can be effected on those inputs by means of
the depicted nonlinear characteristics.
(a) NOT, (b) AND, (c) OR, (d) XOR.
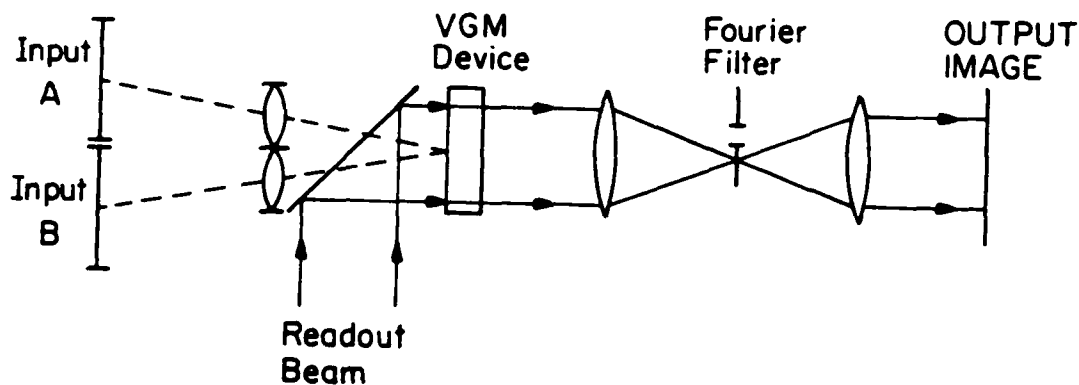
Figure 7. Experimental arrangement for performing logical operations
on two dimensional binary inputs with a VGM device. The
two input images are superimposed on the photoconductor.
The device is read out in transmission. Simple slit
apertures can be used to achieve the desired logic operations.
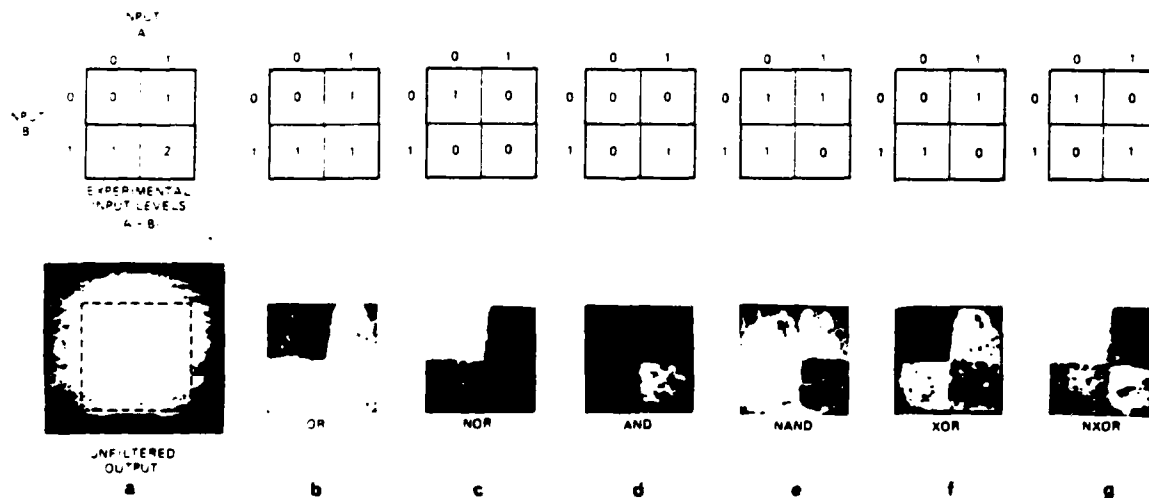

Figure 8. VGM logic results. (a) Two binary images were superimposed
to produce the input intensities on the photoconductor as
shown. Without any filter, the output is ideally a uniform
field (logical 1). The actual output is shown below the
indicated input levels. (b-g) indicate the ideal outputs
and the actual outputs for the logical operations OR, NOR,
AND, NAND, XOR, NXOR, respectively.

Optical logic with variable-grating-mode liquid-crystal devices

P. Chavel,* A. A. Sawchuk, T. C. Strand, and A. R. Tanguay, Jr.

Image Processing Institute, University of Southern California, Los Angeles, California 90007

B. H. Soffer

Hughes Research Laboratories. Malibu. California 90265

A liquid-crystal device that performs a two-dimensional intensity-to-spatial-frequency conversion has been investigated for use as an optical transducer. When such a device is used as the input transducer in an optical filtering arrangement, image-intensity levels can be easily manipulated by using appropriate Fourier plane filters. The variable-grating-mode liquid-crystal device is well adapted to performing binary logic operations on images. Results demonstrating the implementation of common logic operations are presented.

One of the primary concerns in optical image processing and optical computing is the desire for a wider range of real-time input transducers to meet the special requirements of various processing schemes. Variable-grating-mode (VGM) liquid-crystal devices offer a new approach to the problem of optical transducers.[1,2] The basic function of the VGM device is to perform an intensity-to-spatial-frequency conversion over a two-dimensional image field. In this process, the intensity variations of an input image are converted to local spatial-frequency variations in a phase-grating structure within the liquid-crystal layer. As a result of this intensity-to-spatial-frequency conversion, a standard spatial-filtering system can be used to manipulate the VGM spatial frequencies and thus the input intensities.

We describe the application of the VGM device to optical logic operations on binary images. The VGM device permits the implementation of arbitrary nonlinear point transformations of image intensity. The main advantage of the VGM approach over previous methods is the ease of programming the functional nonlinearity desired for a given image transformation. This is accomplished simply by changing the transmittance distribution of the spatial filter in the optical processor. The spatial filter is of relatively low resolution and need only have a space–bandwidth product equal to the number of gray levels to be processed independently of the space–bandwidth product of the input. This programmability advantage applies to the implementation of binary logic operations. One device can be used to implement any of the common logic operations (AND, OR, XOR, and their complements) by simply changing a Fourier plane filter. Previously described optical logic systems were "hard wired" to perform specific operations (see, for example, Refs. 3, 4, and 5). A second major advantage of the VGM system is the possibility of level restoration at each stage, which provides the requisite noise immunity. This capability has been lacking in other numerical processing systems in which noise accumulates in cascaded

stages. Considerable effort has been directed toward using integrated optics for logic elements.[6–8] This approach is inherently one-dimensional and does not exploit the advantages available to fully parallel two-dimensional optical processing algorithms.

The principal element of the variable-grating-mode device is a thin layer of liquid crystal that is observed to form periodic stripe domains in the presence of an applied voltage,[1,2] as shown in Fig. 1(a). The formation of the domains results in a phase grating characterized by a spatial frequency that depends on the magnitude of the voltage across the liquid-crystal layer. The grating period can be optically controlled by placing a
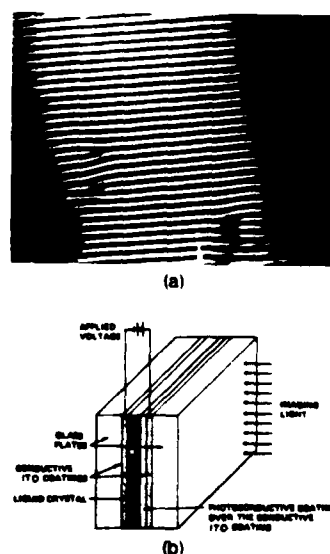

(a)

(b)

Fig. 1. VGM cell. (a) Phase structure viewed through a polarizing microscope. Typical frequencies range from 100 to 500 mm^{-1}. (b) Schematic diagram of the VGM-device construction. At present, devices are read out in transmission at a wavelength at which the photoconductor is insensitive.

two-dimensional photoconductive layer in series with the layer of liquid crystal. The structure of the photoactivated device is shown schematically in Fig. 1(b). The sputter-deposited ZnS photoconductor and the liquid-crystal layer are sandwiched between indium-tin-oxide (ITO) transparent electrodes deposited on glass substrates. To operate the device, a dc drive voltage is impressed across the electrodes. The thin-film structure is designed to accept most of the drive voltage when the photoconductor is not illuminated, such that the fraction of the voltage that drops across the liquid crystal layer is below the activation threshold of the VGM effect. Illumination incident upon a given area of the photoconductive layer reduces its impedance, thereby increasing the voltage drop across the liquid-crystal layer and driving the liquid crystal into its activated state. Thus, because of the VGM effect, the photoconductor converts an input intensity distribution into a local variation of the phase-grating spatial frequency. The high lateral impedance of the thin photoconductive film prevents significant spreading of the photoconductivity and the associated liquid-crystal electro-optic effect. As a result, the light-activation process exhibits high resolution.

To visualize how the VGM device can be used to implement logic operations, one need only realize that the function of a logic circuit can be represented as a simple binary nonlinearity. The input–output characteristics of the common logic functions are shown in Fig. 2. The input in these figures is the simple arithmetic sum of two input image intensities corresponding to logic levels 0 or 1. For example, NOT is simply a hard-clipping inverter, AND and OR are hard-clippers with different thresholds, and XOR is a level slice function. Any spatial light modulator or optical processing system that can produce these nonlinearities can be used for implementing combinatorial logic. Furthermore, if the system allows feedback to be readily introduced, sequential or latching logic can also be implemented. The VGM device is well suited to implementing these nonlinearities. With the VGM approach, nonlinearities are obtained by using a Fourier plane filter whose transmittance variation in one dimension is essentially a plot of the desired nonlinearity. Thus arbitrary nonlinearities are easily produced and changed. Since the nonlinearities associated with logic operations are binary functions, they can be implemented with simple slit apertures, i.e., 0 or 1 transmittance values (Fig. 2). A second feature of the VGM technique that is especially suitable for logic processing is that input image and output beams are physically separate. The input beam modulates a photoconductor; concurrently the image is read out with a second beam. This separation of input and output provides for the possibility of restoring the output levels to the 0 or 1 values even if the input levels are not exactly correct. This feature is essential to the production of a reliable logic system that is immune to noise and systematic errors. Electronic logic elements possess such level-restoring capability, but previously proposed optical logic schemes lack this essential characteristic. Two further aspects of logic operations that are advantageous for optical implementation purposes are that logic operation input levels are discrete and that only a small number (2–4) of distinguishable levels are required. The existence of discrete input levels implies that the nonlinearities need not have the exact forms shown in Fig. 2. In particular, the transition regions need not be perfectly sharp thresholds since the input values are presumed not to occur within the transition regions in any event. The fact that only a few levels need be distinguished implies that the gray-level resolution requirements for the system are minimal. As an additional advantage, the input beam need not be coherent, and output coherence need only be sufficient to distinguish a small number of spatial frequencies. Many logic functions whose implementation would normally require multiple gates can be obtained directly with a single VGM cell. An important example is the full-adder, in which two input bit planes and the carry bit plane are imaged simultaneously onto the VGM device, generating four possible input intensity levels. The four resulting diffracted orders can be filtered to generate the sum bit plane by using the positive orders and simultaneously the carry bit plane by using the negative orders. Thus a full addition can be performed in a single pass through the device. Besides, functions requiring matrix-addressable look-up tables can be generated by utilizing two orthogonally oriented VGM devices in conjunction with a two-dimensional Fourier plane filter. Several such functions are required for optical implementation of residue arithmetic. Finally, in addition to the combinatorial logic functions discussed above, sequential logic may also be implemented with appropriate feedback. In this application, the output plane is imaged onto the input plane. This can be accomplished with incoherent illumination.

A series of experiments was conducted to demonstrate the fundamental logic functions. The experimental setup of Fig. 3 was used. Two input fields were superimposed at the VGM plane along with a bias illumination. The total illumination intensity on the photoconductor of the VGM device was thus the sum of the two input intensities and the bias intensity. The input illumination was a filtered high-pressure mercury-arc lamp. The bias illumination was provided by a tungsten-bulb source. The VGM device was read out in transmission, using a He–Ne laser. Filters were placed in the Fourier plane to select the diffraction orders required in each case. For these experiments, the
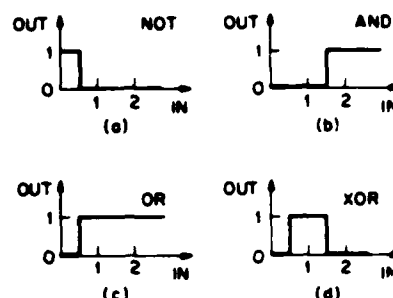

Fig. 2. Logic functions as simple nonlinearities. Given an input consisting of the sum of two binary inputs, different logical operations can be effected by means of the nonlinear characteristics depicted.
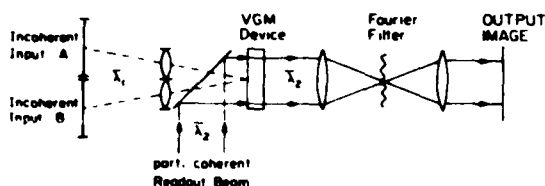
Fig. 3. Experimental arrangement for performing logical operations on two-dimensional binary inputs with a VGM device. The two input images are superimposed on the photoconductor. The device is read out in transmission. Simple slit apertures can be used to achieve the desired logic operations. λ_2 and λ_1 are the mean input and output wavelengths.
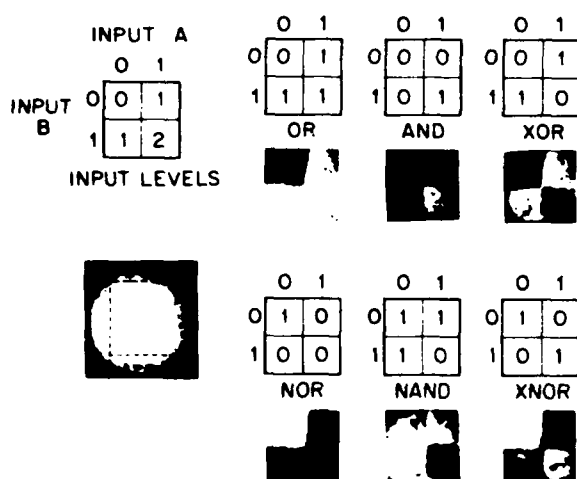

Fig. 4. VGM logic results. At left, two binary images were superimposed to produce the input intensities on the photoconductor as shown. Without any filter, the output is ideally a uniform field (logic 1). The actual output is shown below the indicated input levels. Right, ideal outputs and the actual outputs for the logical operations OR, NOR, AND, NAND, XOR, and XNOR, respectively.

inputs consisted of two rectangular apertures, one vertical and one horizontal. When these were superimposed along with the bias, a square image was formed with the four quadrants having the intensity levels shown in Fig. 4. This image corresponds to the logic truth table shown in the figure. Thus the output images have intensity levels determined by the truth table

associated with the desired logic function. The logic functions AND, OR, XOR, and their complements were implemented sequentially, as shown in Fig. 4, by altering only the Fourier plane filter. Imperfections visible in the output-plane data arise from defects in the cell structure of the VGM device employed in these experiments. Investigations of VGM-device improvements, limitations, processing speed, and pixel uniformity are in progress.

We have described the variable-grating-mode (VGM) liquid-crystal optical transducer, which operates by providing an intensity-to-spatial-frequency conversion. It has been demonstrated experimentally that this device can be used to perform combinatorial logic operations on binary images. Principal among the advantages of the VGM approach is the flexibility of the device inherent in its functional programmability, which may be exercised at will merely by changing a low-resolution spatial filter. Additional advantages include level restoration, fully parallel two-dimensional processing, and reduced coherence requirements.

* Permanent address, Institut d'Optique, Université de Paris Sud, BP 43, 91406 Orsay Cedex, France.

References

1. B. H. Soffer et al., Proc. Soc. Photo-Opt. Instrum. Eng. 218, 81–87 (1980).
2. P. K. Watson, J. M. Pollack, and J. B. Flannery, in Liquid Crystals and Ordered Fluids, J. F. Johnson and R. E. Porter, eds. (Plenum, New York, 1978), Vol. 3, pp. 421–442. See also references therein.
3. R. A. Athale and S. H. Lee, Opt. Eng. 18, 513–517 (1979).
4. S. A. Collins, Jr., U. H. Gerlach, and Z. M. Zakman, Proc. Soc. Photo-Opt. Instrum. Eng. 185, 36–41 (1979).
5. D. H. Schaefer and J. P. Strong III, Proc. IEEE 65, 129–138 (1977).
6. L. Goldberg and S. H. Lee, Appl. Opt. 18, 2045–2051 (1979).
7. S. M. Jensen, Proc. Soc. Photo-Opt. Instrum. Eng. 218, 33–40 (1980).
8. E. Garmire, Proc. Soc. Photo-Opt. Instrum. Eng. 218, 27–32 (1980).

1.8 References

1. Special Issue on Optical Computing, *Proc. IEEE*, vol. 65, January 1977.

2. H. C. Andrews, A. G. Tescher, and R. P. Kruger, "Image Processing by Digital Computer, *IEEE Spectrum*, vol. 9, no. 7, pp. 20-32, 1972.

3. B. R. Hunt, "Digital Image Processing", *Proc. IEEE*, vol. 63, pp. 693-708, 1975.

4. S. H. Lee, "Mathematical Operations by Optical Processing", *Optical Engineering*, vol. 13, pp. 196-107, 1974.

5. J. W. Goodman, *Introduction to Fourier Optics*, McGraw-Hill, New York, 1968.

6. J. W. Goodman, "Operations Achievable With Coherent Optical Information Processing Systems", *Proc. IEEE*, vol. 65, pp. 29-38, 1977.

7. A.A. Sawchuk, et al., "Nonlinear Real-Time Optical Signal Processing," Report USCIPI 900, USC Image Processing Institute, Los Angeles, Ca. 90007, June 15, 1979.

8. B. J. Thompson, "Hybrid Processing Systems – An Assessment", *Proc. IEEE*, vol. 65, pp. 62-76, 1977.

9. D. Casasent, "Spatial Light Modulators," *Proc. IEEE*, vol. 65, pp. 143-157, 1977.

10. S. Iwasa and J. Feinleib, "The PROM Device in Optical Processing Systems", *Optical Engineering*, vol. 13, pp. 235-242, 1974.

11. T. D. Beard, W. P. Bleha, S-Y. Wong, "AC Liquid/Crystal Light Valve", *Appl. Phys. Lett.*, vol. 22, pp. 90-92, 1974.

12. J. Grinberg, et al., "A New Real-Time Non-Coherent to Coherent Light Image Converter", *Optical Engineering*, vol. 14, pp. 217-225, 1975.

13. R. Landauer, "Optical Logic and Optically Accessed Digital Storage," in *Optical Information Processing*, Y.E. Nesterikhin et al. ed., Plenum Press, 1976, pp. 219-253.

14. H.F. Taylor, "Guided Wave Electrooptic Devices for Logic and Computation," *Applied Optics*, vol. 17, pp. 1493-1498, 1978.

15.   L. Goldberg and S.H. Lee, "Integrated Optical Half-Adder Circuit," _Applied Optics_, vol. 18, pp. 2045-2051, 1979.

16.   D.H. Schaefer and J.P. Strong, III, "Tse Computers," _Proc. IEEE_, vol. 65, pp. 129-138, 1977.

17.   R.A. Athale and S.H. Lee, "Development of an Optical Parallel Logic Device and a Half-Adder Circuit for Digital Optical Processing," _Optical Engineering_, vol. 18, pp. 513-517, 1979.

18.   K.Preston, Jr., _Coherent Optical Computers_, McGraw Hill, New York, 1972, ch. 8.

19.   C.C. Guest and T.K. Gaylord, "Two Proposed Holographic Numerical Optical Processors," SPIE Proc. on Optical Processing Systems, vol. 185, pp. 42-49, 1979.

20.   J. Cederquist and S.H. Lee, "The Use of Feedback in Optical Information Processing," _Applied Physics_, vol. 18, pp. 311-319, 1979.

21.   R.P. Akins, R.A. Athale and S.H. Lee, "Feedback in Analog and Digital Optical Image Processing: a Review," SPIE Proceedings, 1979.

22.   S.A. Collins, Jr., U.H. Gerlach and Z.M. Zakman, "Optical Feedback for Generating Arrays of Bistable Elements," SPIE Proc. on Optical Processing Systems, vol. 185, pp. 36-41 1979.

23.   E. Garmire, J.H. Marburger and S.D. Allen, "Incoherent Mirrorless Bistable Optical Devices," _Appl. Phys. Lett._, vol. 32, 320 1978.

24.   B. Kruse, "Experience With a Picture Processor in Pattern Recognition Processing," AFIPS Conf. Proc., vol. 47, pp. 1015-1024 1978.

25.   A. Huang, "The Implementation of a Residue Arithmetic Unit via Optical and Other Physical Phenomena," _IEEE Trans. on Computers_, vol. C-22, pp. 14-18 1973.

26.   A. Huang, Y. Tsunoda, J.W. Goodman, and S. Ishihara, "Optical Computation using Residue Arithmetic," _Appl. Opt._, 18, pp. 149-162 1979.

27.   D. Psaltis and D. Casasent, "Optical Residue Arithmetic: A Correlation Approach," _Appl. Opt._, vol. 18, pp. 163-171, 1979.

28.   F.A. Horrigan and W.W. Stoner, "Residue Based Optical Processor," SPIE Proc., vol. 185, 1979.

29. A. Tai, I. Cindrich, J.R. Fienup, and C.C. Aleksoff, "Optical Residue Arithmetic Computer With Programmable Computation Modules," Appl. Opt., 18, pp. 2812-2823, 1979.

30. S.A. Collins, Jr., "Numerical Optical Data Processor," SPIE Proc. Effective Utilization of Optics in Radar Systems, vol. 128, pp. 313-319, 1977.

31. S.A. Collins, Jr., J. Ambuel and E.K. Damon, "Optics for Numerical Calculation," Proc. ICO-11 Conference, pp. 311-314, Madrid, Spain, 1978.

32. A. Armand, D. Boswell, A.A. Sawchuk, B.H. Soffer and T.C. Strand, "Real-Time Nonlinear Optical Processing with Liquid Crystal Devices," Proceedings 1978 International Optical Computing Conference, London, pp. 153-158, September 1978.

33. A. Armand, D. Boswell, A.A. Sawchuk, B.H. Soffer and T.C. Strand, "Approaches to Nonlinear Optical Processing in Real-Time," Proceedings International Commission for Optics Congress, Madrid, Spain, pp. 253-256, September 1978.

34. A. Armand, D. Boswell, J. Michaelson, A.A. Sawchuk, B.H. r and T.C. Strand, "Real-Time Nonlinear Processing with Halftone Screens," 1978 Annual Meeting, Optical Society of America, San Francisco, October 1978, Journal Optical Society of America, Vol. 68, p. 1361, October 1978.

35. A. Armand, D. Boswell, A.A. Sawchuk, B.H. Soffer and T.C. Strand, "New Methods for Real-Time Nonlinear Optical Processing," 1978 Annual Meeting, Optical Society of America, San Francisco, October 1978, Journal Optical Society of America, Vol. 68, p. 1361, October 1978.

36. A. Armand, A.A. Sawchuk, T.C. Strand, D. Boswell, B.H. Soffer, "Real-Time Parallel Optical Analog-to-Digital Conversion," Optics Letters, Vol. 5, pp. 129-131, March 1980.

37. B.H. Soffer, D. Boswell, A.M. Lackner, A.R. Tanguay, Jr., T.C. Strand, A.A. Sawchuk, "Variable Grating Mode Liquid Crystal Device for Optical Processing," Proceedings Society of Photo-Optical Instrumentation Engineers Los Angeles Technical Symposium – Devices and Systems for Optical Signal Processing, Vol. 218, pp. 81-87, Los Angeles, February 1980.

38. J.D. Michaelson, "A First-Order Model of a Photo-Activated Liquid Crystal Light Valve," Proceedings Society of Photo-Optical Instrumentation Engineers Los Angeles Technical Symposium – Devices and Systems for Optical Processing, Vol. 218, pp. 88-95, Los Angeles, February 1980.

39. J. Michaelson and A.A. Sawchuk, "Nonlinear Optical Processing Using Liquid Crystal Light Valves," Proceedings Society of Photo-Optical Instrumentation Engineers Los Angeles Technical Symposium – Devices and Systems for Optical Signal Processing, Vol. 218, pp. 107-115, Los Angeles, February 1980.

40. B.H. Soffer, D. Boswell, A.M. Lackner, P. Chavel, A.A. Sawchuk, T.C. Strand, A.R. Tanguay, Jr., "Optical Computing with Variable Grating Mode Liquid Crystal Devices," Proceedings Society of Photo-Optical Instrumentation Engineers Technical Symposium East-1980, Optical Computing Conference, Vol. 232, Washington, D.C., April 1980.

41. P. Chavel, A.A. Sawchuk, T.C. Strand, A.R. Tanguay, Jr., B.H. Soffer, "Optical Logic with Variable Grating Mode Liquid Crystal Devices," to appear in Optics Letters, Vol. 5, 1980.

42. A. Armand, "Real-Time Nonlinear Optical Information Processing," Report USCIPI 880, USC Image Processing Institute, Los Angeles, Ca. 90007, June, 1979.

43. A. Armand, A.A. Sawchuk and T.C. Strand, "Nonlinear Optical Processing with Halftones: Accurate Predictions for Degradation and Compensation," to be submitted to Applied Optics.

44. A. Armand, A.A. Sawchuk, T.C. Strand, "Real-Time Parallel Logarithmic Filtering," to be submitted to Applied Optics.

45. S.A. Collins, Jr., M.T. Fatehi, K.C. Wasmundt, "Optical Logic Gates Using a Hughes Liquid Crystal Light Valve," Proc. SPIE Technical Symposium East-Optical Computing Conference, Vol. 232, 1980.

46. J. Michaelson, "Characterization of Liquid Crystal Light Valves and Their Applications to Real-Time Nonlinear Optical Processing," Report USCIPI 930, USC Image Processing Institute, Los Angeles, Ca. 90007, October 1979.

47. S.R. Dashiell and A.A. Sawchuk, "Nonlinear Optical Processing: Effects of Input Medium and Precompensation," Appl. Opt, 16, pp. 2279-2287, 1977.

48. A.A. Sawchuk and S.R. Dashiell, "Nonlinear Coherent Optical Processing – Synthesis Algorithms and Real-time Systems," SPIE Proc. Opt. Info. Proc., Vol. 83, pp. 130-136, San Diego, August 1976.

49. A.A. Sawchuk and T.C. Strand, "Nonlinear Optical Processing," Proc. of Workshop on Future Directions for Optical Information Processing, pp. 26-51, Texas Tech Univ., Lubbock, Texas, May 1980.

50. A.A. Sawchuk and T.C. Strand, "Fourier Optics in Nonlinear Signal Processing," Ch. 9 of *Applications* *of Optical Fourier Transforms*, H. Stark, ed., Academic, New York, to appear (1981).

2. PROFESSIONAL PERSONNEL

The following individuals contributed to the research effort supported by this grant:

1. Alexander A. Sawchuk, Associate Professor, Department of Electrical Engineering, Director - Image Processing Institute, Principal Investigator.

2. Timothy C. Strand, Research Assistant Professor, Image Processing Institute, Senior Investigator.

3. Armand R. Tanguay, Jr., Assistant Professor, Departments of Electrical Engineering and Materials Science, and Image Processing Institute, Senior Investigator.

4. Ahmad Armand, Research Assistant, Ph.D. June 1979, Department of Electrical Engineering. Thesis title: "Real-Time Nonlinear Optical Information Processing."

5. Jerry D. Michaelson, Research Assistant, Ph.D. January 1980, Department of Electrical Engineering. Thesis title: "Characterization of Liquid Crystal Light Valves and their Applications to Real-Time Nonlinear Optical Processing."

6. Pierre H. Chavel, Visiting Research Scientist, Image Processing Institute (on leave from Institut d'Optique, Orsay, France).

7. Robert Forchheimer, Visiting Research Scientist, Image Processing Institute (on leave from Linkoping University, Linkoping, Sweden).

8. Isaiah Glaser, Visiting Research Scientist, Image Processing Institute (on leave from Department of Electronics, Weizmann Institute of Science, Rehovot, Israel).

9. David Drake, Research Assistant, Department of Electrical Engineering.

10. Keith Jenkins, Research Assistant, Ph.D. Candidate, Department of Electrical Engineering.

11. Michael Muha, B.S. June 1979, Department of Physics.

12. Gerard Ashton, B.S. June 1978, Department of Electrical Engineering.

The following individuals have received degrees from the University of Southern California while participating in the research effort:

1. Ahmad Armand, Ph.D., Electrical Engineering, June 1979, thesis title: "Real-Time Nonlinear Optical Information Processing."

2. Jerry Dean Michaelson, Ph.D., Electrical Engineering, January 1980, thesis title: "Characterization of Liquid Crystal Light Valves and Their Application to Real-Time Nonlinear Processing."

3. Gerard Ashton, B.S., Electrical Engineering, June 1978.

4. Michael Muha, B.S., Physics, June 1979.

3. PUBLICATIONS

This section lists written publications resulting from AFOSR support of this project from the initial starting date.

1. A. Armand, D. Boswell, A.A. Sawchuk, B.H. Soffer and T.C. Strand, "Real-Time Nonlinear Optical Processing with Liquid Crystal Devices," _Proceedings 1978 International Optical Computing Conference_, London, pp. 153-158, (September 1978).

2. A. Armand, D. Boswell, A.A. Sawchuk, B.H. Soffer and T.C. Strand, "Approaches to Nonlinear Optical Processing in Real-Time," _Proceedings International Commission for Optics Congress_, Madrid, Spain, pp. 253-256, (September 1978).

3. A.A. Sawchuk and T.C. Strand, "Fourier Optics in Nonlinear Signal Processing," Ch. 9 of _Applications of Optical Fourier Transforms_, H. Stark, ed., to appear, Academic, New York, (1981).

4. A. Armand, D. Boswell, J. Michaelson, A.A. Sawchuk, B.H. Soffer and T.C. Strand, "Real-Time Nonlinear Processing with _Halftone Screens_," 1978 Annual Meeting, Optical Society of America, San Francisco, October 1978, _Journal Optical Society of America_, Vol. 68, p. 1361, (October 1978).

5. A. Armand, D. Boswell, A.A. Sawchuk, B.H. Soffer and T.C. Strand, "New Methods for Real-Time Nonlinear Optical Processing," 1978 Annual Meeting, Optical Society of America, San Francisco, October 1978, _Journal Optical Society of America_, Vol. 68, p. 1361, (October 1978).

6. J. Michaelson, "Liquid Crystal Threshold and Gamma Improvement Using Optical Feedback," submitted for publication to _Optics Letters_.

7. A. Armand, A.A. Sawchuk, T.C. Strand, D. Boswell, B.H. Soffer, "Real-Time Parallel Optical Analog-to-Digital Conversion," _Optics Letters_, Vol. 5, pp. 129-131, (March 1980).

8. A. Armand, A.A. Sawchuk and T.C. Strand, "Nonlinear Optical Processing with Halftones: Accurate Predictions for Degradation and Compensation," to be submitted to _Applied Optics_.

9. A. Armand, A.A. Sawchuk, T.C. Strand, "Real-Time Parallel Logarithmic Filtering," to be submitted to _Applied Optics_.

10. B.H. Soffer, D. Boswell, A.M. Lackner, A.R. Tanguay, Jr., T.C. Strand, A.A. Sawchuk, "Variable Grating Mode Liquid Crystal Device for Optical Processing," Proceedings Society of Photo-Optical Instrumentation Engineers Los Angeles Technical Symposium - Devices and Systems for Optical Signal Processing, Vol. 218, pp. 81-87, Los Angeles, (February 1980).

11. J.D. Michaelson, "A First-Order Model of a Photo-Activated Liquid Crystal Light Valve," Proceedings Society of Photo-Optical Instrumentation Engineers Los Angeles Technical Symposium - Devices and Systems for Optical Processing, Vol. 218, pp. 88-95, Los Angeles, (February 1980).

12. J. Michaelson and A.A. Sawchuk, "Nonlinear Optical Processing Using Liquid Crystal Light Valves," Proceedings Society of Photo-Optical Instrumentation Engineers Los Angeles Technical Symposium - Devices and Systems for Optical Signal Processing, Vol. 218, pp. 107-115, Los Angeles, (February 1980).

13. B.H. Soffer, D. Boswell, A.M. Lackner, P. Chavel, A.A. Sawchuk, T.C. Strand, A.R. Tanguay, Jr., "Optical Computing with Variable Grating Mode Liquid Crystal Devices," Proceedings Society of Photo-Optical Instrumentation Engineers Technical Symposium East-1980, Optical Computing Conference, Vol. 232, pp. 128-136, Washington, D.C., (April 1980).

14. P. Chavel, A.A. Sawchuk, T.C. Strand, A.R. Tanguay, Jr., B.H. Soffer, "Optical Logic with Variable Grating Mode Liquid Crystal Devices," Optics Letters, Vol. 5, pp. 398-400, (September 1980).

15. A.A. Sawchuk and T.C. Strand, "Nonlinear Optical Processing," Proc. of Workshop on Future Directions for Optical Information Processing, pp. 26-51, Texas Tech Univ., Lubbock, Texas, May 1980.

16. A.R. Tanguay, Jr., "Spatial Light Modulators for Real-Time Optical Processing," Proc. of Workshop on Future Directions for Optical Information Processing, pp. 52-77, Texas Tech Univ., Lubbock, Texas, May 1980.

17. B.H. Soffer, J.D. Margerum, A.M. Lackner, D. Boswell, A.A. Sawchuk, A.R. Tanguay, T.C. Strand, and P. Chavel, "Variable Grating Mode Liquid Crystal Device for Optical Processing and Computing," Molecular Crystals and Liquid Crystals, (1981).

18. A.A. Sawchuk, "Nonlinear Real-Time Optical Signal Processing," Proceedings Second SPSE Symposium on Optical Data Display, Processing and Storage, p. 5, Las Vegas, (March 1981).

19. A.A. Sawchuk, "Intensity-to-Spatial Frequency Transformations," Proceeding Society of Photo-Optical Instrumentation Engineers Advanced Institute on Transformations in Optical Signal Processing, Seattle, (February 1981).

20. A.R. Tanguay, Jr., "Real-Time Spatial Light Modulators for Coherent Optical Processing Applications," Proceedings Second SPSE Symposium on Optical Data Display, Processing and Storage, p. 7, Las Vegas, (March 1981).

4. ORAL PRESENTATIONS

This section lists oral presentations at meetings and conferences describing research supported by this grant.

1. A. Armand, D. Boswell, A.A. Sawchuk, B.H. Soffer and T.C. Strand, "Approaches to Nonlinear Optical Processing with Liquid Crystal Devices," presented at the 1978 International Optical Computing Conference, London, (September 1978).

2. A. Armand, D. Boswell, A.A. Sawchuk, B.H. Soffer and T.C. Strand, "Approaches to Nonlinear Optical Processing in Real-Time," presented at the International Commission for Optics Congress, Madrid, Spain, (September 1978).

3. A. Armand, D. Boswell, J. Michaelson, A.A. Sawchuk, B.H. Soffer and T.C. Strand, "Real-Time Nonlinear Processing with Halftone Screens," presented at 1978 Annual Meeting, Optical Society of America, San Francisco, (October 1978).

4. A. Armand, D. Boswell, A.A. Sawchuk, B.H. Soffer and T.C. Strand, "New Methods for Real-Time Nonlinear Processing," presented at 1978 Annual Meeting, Optical Society of America, San Francisco, (October 1978).

5. A.A. Sawchuk, T.C. Strand, A.R. Tanguay, Jr., P. Chavel, D. Boswell, B.H. Soffer, "Parallel Optical Analog-to-Digital Conversion Using a Liquid Crystal Light Valve," Workshop on High Speed A/D Conversion, Portland, Oregon, (February 1980).

6. J.D. Michaelson, "A First Order Model of a Photo-Activated Liquid Crystal Light Valve," presented at SPIE Los Angeles Technical Symposium-Devices and Systems for Optical Processing, Los Angeles, (February 1980).

7. B.H. Soffer, D. Boswell, A.M. Lackner, A.R. Tanguay, Jr., T.C. Strand, A.A. Sawchuk, "Variable Grating Mode Liquid Crystal Device for Optical Processing," presented at SPIE Los Angeles Technical Symposium-Devices and Systems for Optical Processing, Los Angeles, (February 1980).

8. J.D. Michaelson and A.A. Sawchuk, "Nonlinear Optical Processing Using Liquid Crystal Light Valves," presented at SPIE Los Angeles Technical Symposium-Devices and Systems for Optical Processing, Los Angeles, (February 1980).

9. B.H. Soffer,   D. Boswell,   A.M. Lackner,   P. Chavel,
A.A. Sawchuk, T.C. Strand, A.R. Tanguay, Jr., "Optical Computing
With Variable Grating Mode Liquid Crystal Devices," SPIE
Technical Symposium East-1980 Optical Computing Conference,
Washington, D.C., (April 1980).

10. A.A. Sawchuk, T.C. Strand, A.R. Tanguay, Jr., P. Chavel,
D. Boswell, A.M. Lackner and B.H. Soffer, "Variable Grating Model
Liquid Crystal Light Valves and their Application to Optical
Processing," Gordon Research Conference on Coherent Optics and
Holography, Santa Barbara, California, June 1980.

11. B.H. Soffer, D. Boswell, A.M. Lackner, A.R. Tanguay, Jr.,
T.C. Strand, A.A. Sawchuk, "Variable Grating Mode Liquid Crystal
Devices for Optical Processing and Computing," Eighth
International Liquid Crystal Conf., Kyoto, Japan, June 1980.

12. A.A. Sawchuk,   "Nonlinear   Real-Time   Optical   Signal
Processing," Second SPSE Symposium on Optical Data Display,
Processing and Storage, Las Vegas, March 1981.

13. A.A. Sawchuk,   "Intensity-to-Spatial   Frequency
Transformations," SPIE Advanced Institute on Transformations in
Optical Signal Processing, Seattle, February 1981.

14. A.R. Tanguay, Jr., "Real-Time Spatial Light Modulators for
Coherent Optical Processing Applications," Second SPSE Symposium
on Optical Data Display, Processing and Storage, Las Vegas, March
1981.

END

DATE
FILMED

10-81

DTIC